Opposing effects of calcium stress in human muscle: defective glucose utilization leading to diabetes vs. stress-adaptive effects of a junctophilin fragment

Eshwar R. Tammineni[1], Lourdes Figueroa[1], Carlo Manno[1], Natalia Kraeva[2], Carlos A Ibarra[2], Amira Klip[3], Sheila Riazi[2] and Eduardo Ríos[1]

[1]Department of Physiology and Biophysics, Rush University, Chicago, United States; [2]Department of Anesthesia & Pain Management, University of Toronto; [3] Cell Biology Program, The Hospital for Sick Children, Toronto, Canada.

Address for correspondence:

Eduardo Ríos

Rush University School of Medicine

1750 West Harrison Street, Suite 1279 JS

Chicago, IL 60612, USA

Erios@rush.edu

Ph. 312 9422081 (office), 312 9426454 (Department)

312 2868261 (cell). Fax 312 9428711

Abstract

Contraction of striated muscle, which is controlled by movements of calcium ions between cellular stores (SR) and cytosol, is the function consuming the most energy in mammals, which also makes muscle the main user of circulating glucose and regulator of its level. Accordingly, inadequate removal of glucose by muscle is the main proximate cause of hyperglycemia, leading to insulin resistance and diabetes. Multiple diseases of muscle course with chronically elevated cytosolic calcium. Here we show in a sample of malignant hyperthermia-susceptible (MHS) patients, a significant decrease in content of junctophilin1, an essential protein of the couplon —the supramolecular device that effects calcium release from the SR— accompanied by an increase in a 44 kDa C-terminal junctophilin fragment, JPh44, and the activating cleavage of GSK3β, a specialized kinase that inhibits glycogen synthase. We trace these changes to activation, by the excess calcium, of calpain1, a serine/threonine kinase. By high-resolution imaging of antibody markers or fluorescent probes expressed in patients' and murine muscle and patient-derived and C2C12 myotubes, we demonstrate detailed colocalization of junctophilin1 with the calcium channel RyR1, marking the couplon, and of calpain1 with both. We also show that the JPh44 fragment moves away from the couplon and into nuclei, a movement greatly increased in MHS. Cultured myotubes expressing a JPh44-like construct had altered gene transcription in multiple pathways, including changes that promote glucose utilization. Together with less transcription, the expression of GSK3β was reduced, which predicts increased glucose utilization. In summary, the changes observed in these patients add to the wide-ranging alterations in metabolism that eventually lead to hyperglycemia and diabetes, assign the changes to proteolysis by calcium-activated calpain1, and reveal the production and beneficial, stress-adaptive function of a novel regulator of transcription, JPh44. Similar stress-adaptive roles have been described for a junctophilin2 fragment in heart failure.

Alternative Abstract (200 words)

Calcium ion movements between cellular stores and the cytosol govern muscle contraction, the most energy-consuming function in mammals, which confers striated myocytes a pivotal role in glycemia regulation. Chronic myoplasmic calcium elevation, found in malignant hyperthermia-susceptible (MHS) patients and in other myopathies, has been suggested to underlie the progression from hyperglycemia to insulin resistance. However, what drives such progression remains elusive. We find that muscle cells derived from MHS patients have decreased content of junctophilin1, a protein that colocalizes in the couplon with both the calcium channel RyR1 and calpain1, accompanied by an increase in a 44 kDa junctophilin1 fragment (JPh44) that localizes in the nuclei. We also find increased an activated fragment of GSK3β — a specialized kinase that inhibits glycogen synthase, which favors glycogenolysis. We trace these changes to activated proteolysis by calpain1, secondary to increased myoplasmic calcium. We demonstrate that a JPh44-like construct induces transcriptional changes predictive of increased glucose utilization in myotubes, including decreased translation of GSK3β. These effects reveal a stress-adaptive response, similar to that of a junctophilin 2 fragment described in heart failure, mediated by the novel regulator of transcription JPh44.

Introduction

In the excitation-contraction (EC) coupling process of striated muscles, action potential depolarization of the plasma or transverse (T) tubule membranes command the transient release of Ca^{2+} into the myoplasm, enabling muscle contraction. The crucial device in this process is the couplon, a physical continuum of proteins that includes dihydropyridine receptor (DHPR), ryanodine receptor 1 (RyR1), FKBP12, junctophilin 1 (JPh1), Stac3, Junctin, Triadin and Calsequestrin, among other components (1,2).

Only 5 proteins are necessary to assemble a functional, skeletal muscle-type EC coupling system in expression models (3,4). One of them is junctophilin, JPh (5), with skeletal and cardiac isoforms (1 and 2) deemed essential for creating and maintaining the junctional structure (dyads and triads) characteristic of striated muscle(6,7).

Susceptibility to Malignant Hyperthermia (MHS(8)) is a condition paradigmatic of gain-of-function couplonopathies (9,10). The primary defect in MHS is an alteration of RyR1 or another couplon protein, which leads to an increase in resting or activated openness of the channel. The increased "leak" causes a reduction in Ca^{2+} content and free ion concentration inside the SR, in turn leading to an increase in resting free Ca^{2+} concentration, $[Ca^{2+}]_{cyto}$ (11,12), secondary to changes in the plasma membrane in response to SR depletion (13–16). Duchenne Muscular Dystrophy (DMD) is another example of a condition that raises resting $[Ca^{2+}]_{cyto}$, albeit by different mechanisms (17–19)

MHS patients show other abnormalities, probably derived in many cases from the chronically elevated $[Ca^{2+}]_{cyto}$. They have altered musculoskeletal function (with pain, cramps, stiffness, muscle fatigue and bone deformity as common manifestations(20,21)), and systemic dysfunction. Notably, and possibly as a consequence of reduced uptake and processing of glucose by muscle(22), the frequency of hyperglycemia(23) and diabetes(22) is more than 2-fold greater in MHs patients than in the general age-matched population.

In cardiac muscle, the junctophilin isoform JPh2 is known to have a similar function as JPh1 in skeletal muscle, in maintaining structural integrity of the t-SR junction or dyad(24). Strikingly, fragments of JPh2 have been shown to additionally work in regulation of gene expression within nuclei(25,26).

We now demonstrate that the content of full-size JPh1 is reduced in skeletal muscle of MHS patients, while a C-terminal 44-kDa JPh1 fragment, which we refer to as JPh44, moves away from the triadic location of the full-size protein and relocates to the nucleus. The observations indicate that the increased cleavage of JPh1 in MHS patients is due to activation of calpain1 by their higher $[Ca^{2+}]_{cyto}$.

We also show that the JPh44 fragment contains the C-terminus of JPh1, and includes sequences that allows it to enter nuclei and interact with DNA.

The proteolysis of JPh1, with possible de-stabilization of T-SR junctions (6,27), and the entry of its fragments into nuclei could contribute to the disease phenotype, as proposed for fragments of JPh2 produced in cardiac muscle of failing hearts (26). On the other hand, Guo et al. (25) provided evidence that the intra-nuclear actions of JPh2 fragments are "stress-adaptive", partially offsetting the negative consequences of activation of proteolysis.

Given these precedents and the presence in the sequence of JPh44 of segments capable of interaction with DNA, here we also tested the hypothesis that JPh44 exerts transcriptional control that tends to compensate for the deleterious effects of elevated $[Ca^{2+}]_{cyto}$. The study demonstrates beneficial effects of the fragment on the transcription and translation of enzymes active in glucose utilization by skeletal muscle.

Results

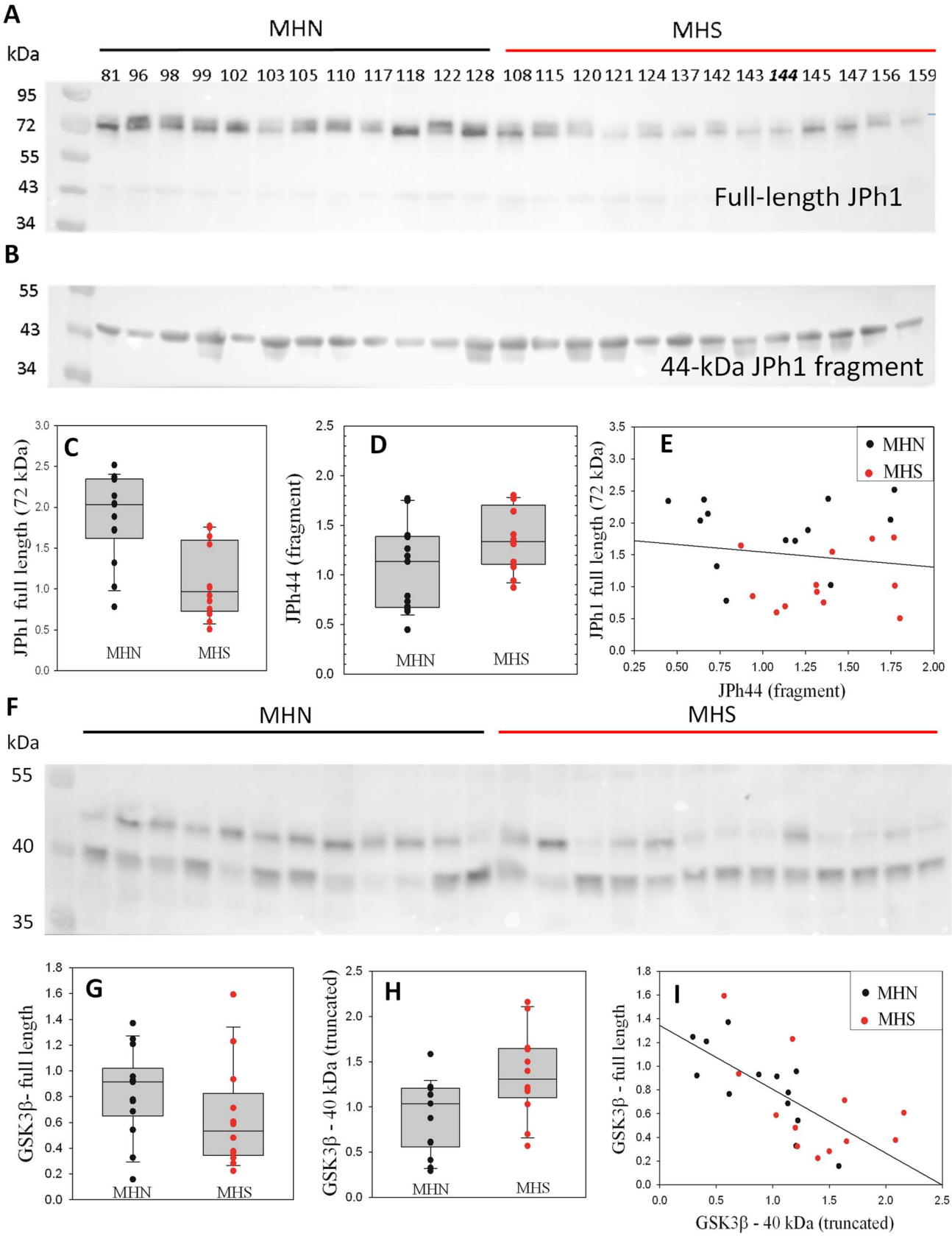
A
MHN
MHS
kDa
81 96 98 99 102 103 105 110 117 118 122 128 108 115 120 121 124 137 142 143 144 145 147 156 159
95
72
55
43
34
Full-length JPh1
B
55
43
34
44-kDa JPh1 fragment
C
JPh1 full length (72 kDa)
MHN
MHS
D
JPh44 (fragment)
MHN
MHS
E
JPh1 full length (72 kDa)
JPh44 (fragment)
MHN
MHS
F
MHN
MHS
kDa
55
40
35
G
GSK3β- full length
MHN
MHS
H
GSK3β - 40 kDa (truncated)
MHN
MHS
I
GSK3β - full length
GSK3β - 40 kDa (truncated)
MHN
MHS

Figure 1. Fragmentation of proteins in MHS human muscle. A, Western blot (WB) of whole protein fraction from patients' muscle biopsies, stained with "antibody A", which preferentially marks full-length junctophilin (JPh1). Patients were diagnosed as MHN or MHS as indicated. Numbers identify individuals. B, WB of same gel, using "antibody B", which preferentially stains JPh44. C, D, box plots of signal in the 13 MHN and 12 MHS bands of panels A and B, respectively. p of no difference is <0.001 and 0.06, respectively for JPh1 and JPh44. E, JPh1 vs JPh44 WB signals for all patients. The correlation is negative and poor (R = 0.16). F, WB of whole protein fraction from the same biopsies, stained for GSK3β. G, H, box plots of the signal in the ~47 and ~40 kDa bands for MHN and MHS patients. The difference is highly significant for the light band signal (p = 0.015) but not for the 47 kDa band (p = 0.14). I, 40 kDa vs. 47 kDa signals for all patients. The correlation is negative and highly significant (R = 0.69, p < 0.001). Data trace. Raw data and statistical calculations in *GSK3β graphs and statistics.JNB*, sections 1 and 2.

JPh1 is cleaved in MH-susceptible patients

A large increase in $[Ca^{2+}]_{cyto}$ has been found in muscle fibers from MHS individuals (12), myotubes derived from MHS patient biopsies (21) and in MHS animals (11). MHS animals also showed increased calpain activity (28). Given that junctophilins are targets of Ca^{2+}-activated calpain proteases (25,26), we hypothesized that excess $[Ca^{2+}]_{cyto}$, by promotion of calpain activity, enhances JPh1 cleavage in MHS individuals. As a test, JPh1 was quantified by Western blotting (WB), on the same 25-lane gel, total protein extracts from biopsied muscle of 13 MHN (normal) and 12 MHS subjects. The immunoblot, stained using an antibody referred to here as "A", is shown in Fig. 1A. A visible reduction in the MHS of a ~72 kDa stained band corresponding to the full size JPh1, revealed an almost 2-fold, statistically significant difference in content (Fig. 1C). A blot from a different gel, stained with a different anti-JPh1 antibody — "B"— showed a greater content of a band with an effective migration size of ~44 kDa, referred to as JPh44 (Fig. 1B). The excess content of this fragment in MHS (quantified in Fig. 1D) was marginally significant.

While these results would imply that a greater cleavage of JPh1 leads to a reduction in its content, with consequent increase in the content of its fragments, there is a poor negative correlation in individual subjects between these two changes (Fig. 1E). The tentative conclusion from this observation is that the cleavage process, which may operate in multiple sites and sequentially on cleaved products, blurs any detailed correspondence between increase in content of a given fragment and disappearance of the full-size protein.

The study leads to another conclusion: in Fig. 1A, antibody A is seen to barely mark the presence of the 44 kDa fragment. This relative specificity for the full-size protein proved especially useful to distinguish it from its fragments in images of adult muscle. By contrast, antibody B stains specifically JPh44 (supplemental Fig. 1 to Fig. 1). Additional information on provenance and reactivity of antibodies A and B is given in Methods.

Fragmentation of glycogen synthase kinase 3 (GSK3) is increased in MHS patients

In previous work (22) we demonstrated that phosphorylase kinase (PhK), an enzyme that reciprocally activates glycogen phosphorylase (GP) and inhibits glycogen synthase (GS), is activated in the muscle of MHS patients, effects consistent with an observed shift of the glycogen ←→glucose balance towards glycogenolysis (22), which is presumed responsible for the hyperglycemia and diabetes that develops in many of these patients (22,23). Here we compared the contents of GSK3β, a serine/threonine protein kinase that directly inhibits GS by

phosphorylation. The kinase activity of GSK3β is controlled by its phosphorylation at Ser 9, and is also promoted by truncation of the original ~47 kDa molecule to a form of ~40 kDa (29–31).

WB of protein extracts (Fig. 1F) from muscle biopsies of the same patients of Fig. 1A, reveal both forms of GSK3β. The signal in the 47 kDa band of full-size GSK3β was reduced in MHS, while that of the activated 40 kDa fragment was increased. The changes in the two proteins were highly negatively correlated (Fig. 1I); consequently, the ratio of signals (40 kDa/47 kDa) was more than 3-fold greater in the MHS group, with high statistical significance. Regardless of diagnosis (MHS or MHN), there was a significant positive correlation between content of the activated GSK3β form and serum glucose (supplemental Fig. 2 to Fig. 1). These results are consistent with activation of the GS kinase by calpain proteolysis, which contributes to the shift in glycogen ←→glucose balance in favor of glycogenolysis, presumably by inhibitory phosphorylation of GS.

Localization of JPh1-44 fragment in skeletal muscle

In cardiac muscle, the full-length JPh2 protein is located at terminal cisternae of the SR, while cleaved JPh2 fragments can be found inside nuclei (25,26). Here we defined the location of JPh1 and JPh44 using immunostaining with site-specific JPh1 antibodies combined with 3D high resolution-imaging, a procedure used for every fluorescence image shown in this study, consisting in acquisition of vertical "z-stacks" of confocal 2D images, followed by a correction algorithm (described in Methods). Moderately stretched thin myofiber bundles were fixed in PFA and differentially stained with antibody A, already used in fig. 1A and shown to specifically mark full-length JPh1. Other bundles were stained with antibody B, demonstrated with supplemental Fig. 1 to Fig. 1 to react solely to the 44-kDa fragment. As shown in Fig. 2, JPh1 (panels Aa-Ad) was always present at T-SR junctions, where it was highly colocalized with RyR1. In contrast, antibody B located the JPh44 fragment as discrete particles at variable locations within the sarcomeric I band, as well as nuclei (panel 2Bb), and accordingly failed to colocalize with Ry1 (panels 2Cc, Cd).

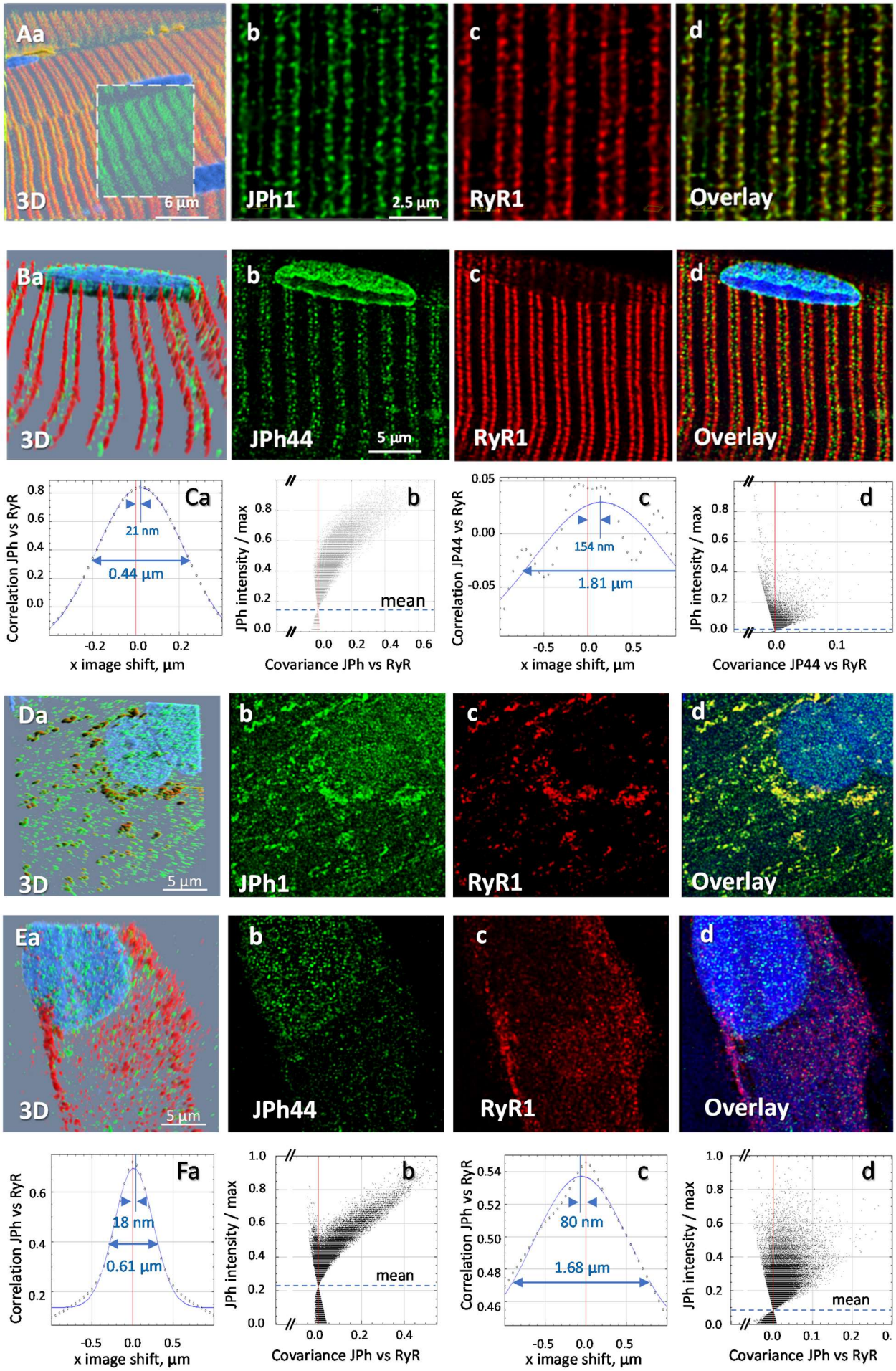
Aa
3D
6 µm
b
JPh1
2.5 µm
c
RyR1
d
Overlay
Ba
3D
b
JPh44
5 µm
c
RyR1
d
Overlay
Ca
Correlation JPh vs RyR
21 nm
0.44 µm
x image shift, µm
b
JPh intensity / max
mean
Covariance JPh vs RyR
c
Correlation JP44 vs RyR
154 nm
1.81 µm
x image shift, µm
d
JPh intensity / max
Covariance JP44 vs RyR
Da
3D
5 µm
b
JPh1
c
RyR1
d
Overlay
Ea
3D
5 µm
b
JPh44
c
RyR1
d
Overlay
Fa
Correlation JPh vs RyR
18 nm
0.61 µm
x image shift, µm
b
JPh intensity / max
mean
Covariance JPh vs RyR
c
Correlation JPh vs RyR
80 nm
1.68 µm
x image shift, µm
d
JPh intensity / max
mean
Covariance JPh vs RyR

Figure 2. Location of two forms of junctophilin in human skeletal myofibers and myotubes: A, B, Images of full-length JPh1 and JPh44, respectively stained with antibodies "A" and "B", in cells co-stained for RyR1. Full-length JPh1 and Ryr1 (panels Ab, c) are highly overlapping at T-SR junctions. JPh44 moves away into the I band (panels Bb, d). Colocalization between JPh1 and RyR1 is high, as demonstrated by the Van Steensel's and Li's analyses (panels Ca, b), leading to 4 measures (R, VS shift, FWHM and ICQ) listed in Table 1. As indicated in Ca, VS shift is 21 nm and FWHM is 0.6 µm. Colocalization of JPh44 and RyR2 is lost, as indicated by a VS shift of 58 nm, a FWHM of 1 µm defined on a Gaussian that fits poorly an oscillating VS plot and a Li plot characteristic of no colocalization and exclusion (compare panels Cb and Cd). D, E, primary myotubes derived from patients' muscle, stained respectively with antibodies A and B, and co-stained for RyR1. Note in panels D, overlap of antibody A fluorescence, largely marking JPh1 with cytosolic RyR1. In E, antibody B fluorescence, which marks JPh44, is largely intra-nuclear, with no colocalization with RyR1. Visual impression is supported by colocalization analyses (panels F, replication results in Table 1). Data trace. Average colocalization measures are listed in Table 2. Experiment identifiers: panel A, 102919La Series 010; panel B, 102519L Series 018; panels D, G, 072420Lb Series 002; panel E, 030120Lb Series 001. Statistics of location in Table 2. Data in Summary ratios.xlsx, main.

Colocalization between the junctophilin forms and RyR1 in patient's muscles was quantified by four measures, with average results listed in Table 1. First: R, Pearson's correlation coefficient of immunofluorescence intensities, calculated pixel by pixel after subtraction of a small background signal. This index had high value for JPh1 (represented by antibody A fluorescence) and low for JPh44 (antibody B), with high statistical significance of the difference. Second: the Intensity Correlation Quotient (ICQ), emergent from an approach by Li et al. (32) illustrated in panel 2Cb, whereby the intensity of fluorescence of antibody A (JPh1) is plotted, pixel by pixel, against the covariance of antibody A and RyR1 intensities (Methods). The comma-shaped cloud with negative curvature, shown in 2Cb, is a characteristic of high colocalization, contrasting with the funnel-shaped cloud found for antibody B vs RyR1 (panel 2Cd), which includes pixels with negative covariance, reflecting mutual exclusion rather than colocalization. The ICQ, which varies between -0.5 (reflecting exclusion) and 0.5 (perfect colocalization), was close to 0.5 for antibody A, while that of antibody B was smaller but still positive, a difference with high statistical significance (Table 1; here and elsewhere significance was established through replications).

A third approach, introduced by Van Steensel et al. (33) and illustrated in Fig. 2Ca, c, plots the correlation coefficient of the two signals, averaged over all pixels, vs. a variable shift of one of the images in one direction (in the example, the shift is in the x direction, parallel to the fiber axis). The curve generated is then fitted by a Gaussian. The x-axis location of the apex of the Gaussian (or that of the actual correlation, when the fit is poor), named "VS shift", provides a rough measure of the average separation of the two fluorescent species in the x direction. In the example, the distance was 21 nm for JPh1 (antibody A, panel 2Ca) and 154 nm for JPh44 (2Cc), a significant difference (Table 1). The FWHM of the fitted Gaussian is a second measure of dispersion or de-localization, also greater for the JPh fragment. Further use of these techniques will show that the calculation of 4 different measures provides a multidimensional view of colocalization — or its absence — revealing differences between proteins and treatments not reflected in the usual correlation analysis.

Images of patient-derived primary myotubes, stained with antibodies A and B and co-stained for RyR1, are illustrated in Fig. 2 D, E). Here too, the differences were clear. Antibody A staining in cytosol was highly colocalized with RyR1 (2D, 2F, quantification in Table 1), in clusters that presumably correspond to developing junctions. In agreement with the observation in myofibers, antibody B did not colocalize with RyR1 and was found

mostly within nuclei (panel 2Eb), in fine granular form. Unlike myofibers, myotubes had some intra-nuclear staining with antibody A, which adopted a fine granular pattern similar to that of antibody B. Rather than entry of JPh1 into nuclei, observations presented later indicate that intranuclear antibody A reflects reactivity to JPh44 occurring in myotubes but not in adult muscle.

The 44-kDa fragment internalized in nuclei includes the C terminus of JPh1

In earlier studies of JPh2, both N-terminal (25) and C-terminal fragments(26) were shown to translocate to nuclei, in conditions of heart stress. To identify the JPh1 segment cleaved as JPh44 and follow its movements, a fusion of JPh1 with GFP (at the N terminus) and the FLAG tag (at the C terminus) was expressed in myotubes, derived from patients' muscle or a C2C12 line, and in mouse adult myofibers. Panels A and B in Fig. 3 show GFP fluorescence in myotubes expressing GFP-JPh1-FLAG (green) largely in the cytosol, in the form of small clusters or puncta. Instead, the C-terminal FLAG (red) appeared in both nuclear and extra-nuclear regions — corresponding to the cytosol and other organelles. Within the latter, the FLAG tag was distributed in two forms: punctate, colocalized with (N-terminal) GFP fluorescence, as well as a finely particulate disperse form, away from GFP.

The asymmetry was quantified by the ratio of signal densities, extra-nuclear (loosely called cytosolic)/nuclear, which in C2C12 myotubes was approximately 3-fold greater for GFP, a highly significant difference (Table 2). When the plasmid was expressed in myotubes derived from human muscle, a difference greater than 2-fold, again in favor of GFP, was found (panels 3B and Table 2). A clear nuclear internalization of FLAG, with exclusion of GFP, was also found in adult mouse muscle expressing the plasmid (Fig. 3C). In this case the ratio (cytosolic/nuclear) of signal densities was nearly 1000-fold greater for the N-terminal GFP than for the C-terminal FLAG (Table 2).

An additional observation (illustrated with panels 3Ca, d, e and repeated in replications) was that in myofibers of adult mice the C-terminal fragment accumulated in perinuclear regions, in addition to entering nuclei. This was not the case for the native JPh44 in myofibers (Fig. 2), which suggests that the perinuclear buildup may be a consequence of the steep gradient generated by the transient increase of concentration of the fragment, combined with a diffusion barrier at the nuclear membrane. Myotubes do not show a similar accretion (Fig. 3Ad, Bd), which suggests either a slower production of the protein or a lower barrier to nuclear entry.

In the transfected mouse myofibers we also found the N-terminal GFP strictly colocalized with endogenous RyR1 at triads, reproducing the colocalization of endogenous JPh1 and RyR1 found in human myofibers (illustrated with Fig. 7). These observations allow the following conclusions: in both developing and adult tissue, the full-size protein is attached to junctions between plasma or T membrane and SR; the C terminus is part of the cleaved fragment that migrates into the I band and enters nuclei; the N terminus of JPh1 stays with the plasma or T membrane, whether as part of the full protein or after cleavage.

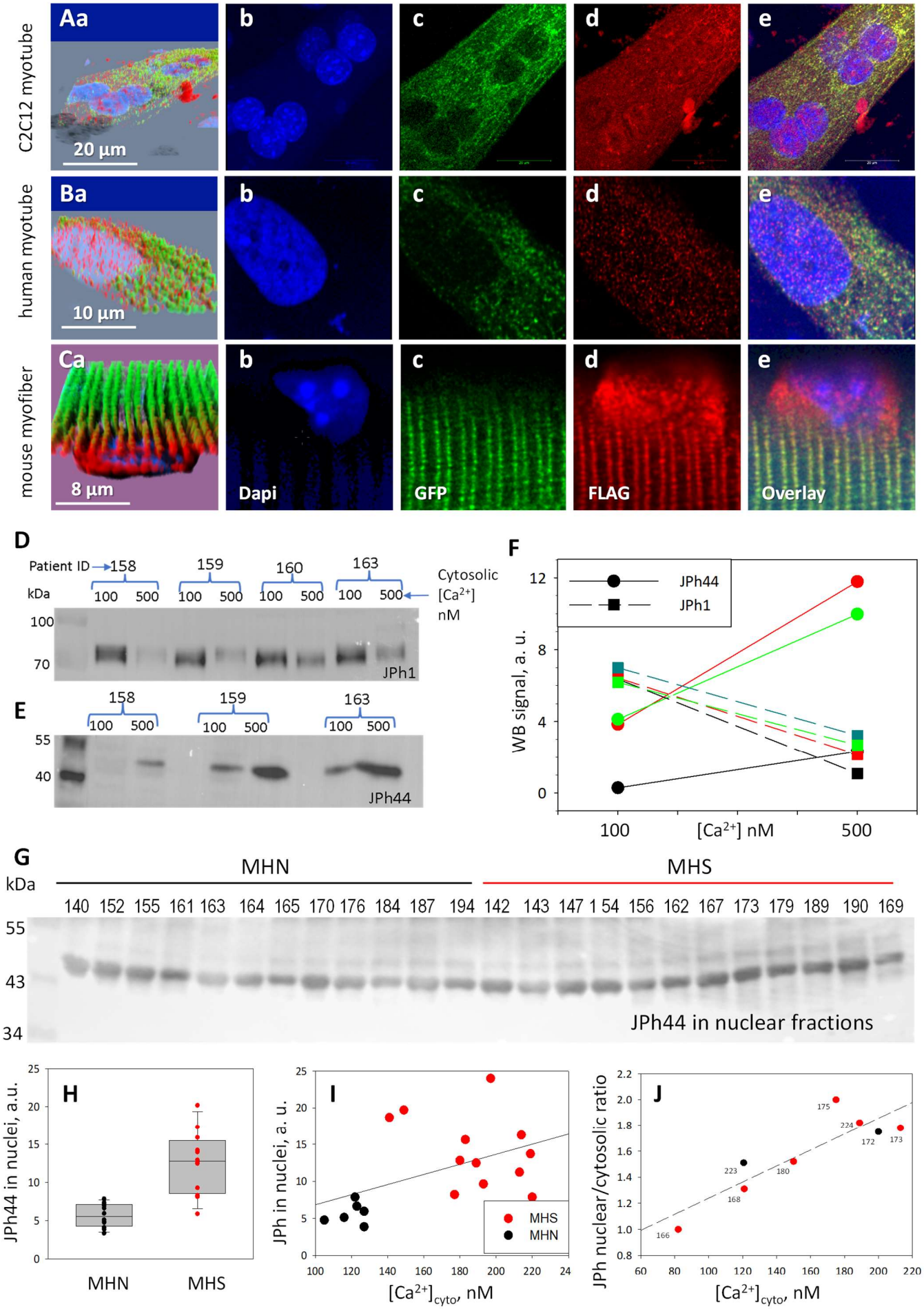
C2C12 myotube
human myotube
mouse myofiber
Aa
b
c
d
e
20 µm
Ba
10 µm
Ca
8 µm
Dapi
GFP
FLAG
Overlay
D
Patient ID
158
159
160
163
kDa
100
500
Cytosolic [Ca2+] nM
100
70
JPh1
E
55
40
JPh44
F
JPh44
JPh1
WB signal, a. u.
[Ca2+] nM
G
MHN
MHS
kDa
140 152 155 161 163 164 165 170 176 184 187 194 142 143 147 1 54 156 162 167 173 179 189 190 169
55
43
34
JPh44 in nuclear fractions
H
JPh44 in nuclei, a.u.
MHN
MHS
I
JPh in nuclei, a. u.
[Ca2+]cyto, nM
J
JPh nuclear/cytosolic ratio
[Ca2+]cyto, nM

Figure 3. Distribution of a dually tagged JPh1 and its fragments. A-C, confocal images of cells expressing the (N)GFP-JPh1-FLAG(C) construct. In myotubes (A, B), GFP is exclusively in the cytosol, while FLAG, marking the full-size protein and its C-terminal fragment(s), red, distributes widely, including inside nuclei. The different distribution is also evident when the construct is expressed in adult muscle (panels C), with the additional observation of accumulation of the N-terminal fragment in perinuclear regions (Cd). Panels Aa, Ba and Ca provide a 3D view of the z-stack of images, showing the intracellular location of the FLAG mark. The distribution differences are highly statistically significant (Table 3). D-F, effect of extracellular Ca^{2+} on JPh1 content of permeabilized muscle from 4 patients. WB of whole tissue protein of muscles exposed to 100 or 500 nM [Ca^{2+}] stained with antibody A (marking the full-size JPh1, panel D) or B (marking JPh44, panel E). The normalized signals, plotted in F, show reciprocal changes of content in high [Ca^{2+}]. G, JPh44 (stained with antibody B) in whole muscle nuclear fraction extracted from 12 MHN and 12 MHS individuals. H, the average content is more than 2-fold greater in MHS ($p < 0.001$). I, JPh44 content in nuclei (from WB in panel G) vs. $[Ca^{2+}]_{cyto}$ in primary myotubes from the same muscle samples, showing a statistically significant positive correlation ($R = 0.48$, $p = 0.04$). J, ratio JPh content in nuclei / JPh in cytosol, in images of myotubes stained with antibody A, vs. $[Ca^{2+}]_{cyto}$. The correlation is positive and statistically significant ($R = 0.88$, $p = 0.004$). Data trace. A: experimental record 091620a Series 5 Lng; B: 091020a Series 4 Lng, from patient MHN #179; C: 100520a Series 2. F H I J in *JPh vs Ca and GSK3b vs FSB.JNB*. F in Section 1, I in Section 2, J in Section 3.

Elevated cytosolic calcium concentration mediates the increase in JPh1 cleavage

Resting $[Ca^{2+}]_{cyto}$ in myofibers of MHN and MHS human subjects was reported as 112 nM and 485 nM, respectively (12). Hypothesizing that the increased cleavage of JPh1 in MHS subjects is associated with increased $[Ca^{2+}]_{cyto}$, we recorded the effect of experimentally elevated cytosolic [Ca^{2+}], to levels consistent with the MHS patients mentioned above, on the fragmentation of JPh1. Biopsied myofiber bundles from three patients, pinned in chambers and exposed to saponin for permeabilization, were superfused with either 100 or 500 nM [Ca^{2+}]. After 10 min of exposure, the bundles were processed separately to extract protein (hereon whole-protein extracts). Quantitative Western blotting of the extract found increased JPh1 cleavage upon exposure to higher [Ca^{2+}] (Fig. 3 D-F).

Together with an excess JPh44 in whole-protein extracts from MHS patients' muscle, we found a significantly higher JPh44 content in nuclear fractions from these biopsies (Fig. 3G, H). The altered phenotype of MHS patients, including elevated $[Ca^{2+}]_{cyto}$, is reproduced to a large extent in myotubes derived from their muscle biopsies (21,34). Two remarkable observations affirm the relevance of the elevated cytosolic calcium in defining the altered phenotype. First, there was a positive correlation between the nuclear JPh44 content in the muscle of patients and $[Ca^{2+}]_{cyto}$ in their derived myotubes (Fig. 3I). There was also a significant positive correlation between nuclear content of JPh in the myotubes (as quantified by the nuclear/cytosolic ratio of JPh densities) and their $[Ca^{2+}]_{cyto}$ (Fig. 3J). Taken together, the observations indicate that cleavage of JPh1 and nuclear internalization of the 44 kDa fragment increase in MHS muscle, driven by the higher $[Ca^{2+}]_{cyto}$ found in these patients.

Calpain1 cleaves JPh1 in T-SR junctions

JPh2 in mammalian heart is cleaved by calpains (25,26), most effectively by calpain1, a heterodimer that incudes a main (~80 kDa) subunit (35). Calpain1 activates in the presence of [Ca^{2+}] in the 50-300 nM range, an activation associated with autolysis to a ~76 kDa isoform resulting from cleavage of 27 residues at the N terminus (36–38). We hypothesized that calpain1 is largely responsible for the increased cleavage of JPh1 in MHS.

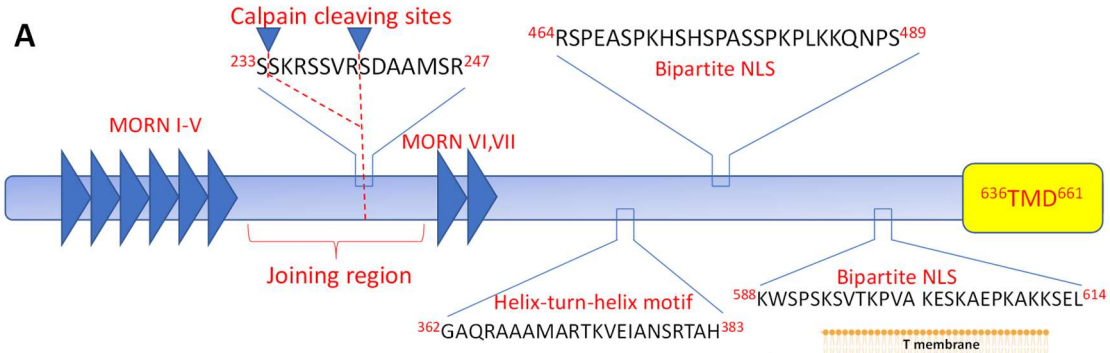

B

Position of cleavage	Amino acid sequence	Score
240	SISSKRSSVR|SDAA	1.481
233	RKSESKSSIS|SKRS	1.402
484	SPASSPKPLK|KQNP	1.307
478	SPKHSHSPAS|SPKP	1.234
582	SSQSSSALVH|KPSA	1.215

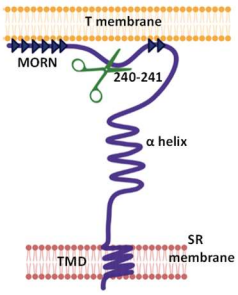

D

UniprotKB	Species	Position of cleavage	Amino acid sequence	GPS-CCD score
Q9HDC5	Human	240	...ESKSSISSKRSSVR|SDAAMSR...	1.481
Q9ET80	Mouse	240	...ESKSSISSKRSSVR|SDAAMSR...	1.481
D3ZQ55	Rat	240	...ESKSSISSKRSSVR|SDAAMSR...	1.481
E2R0Z6	Dog	240	...ESKSSISSKRSSVR|SDAAMSR...	1.481
A0A6P7ECH9	Sheep	240	...ESKSSISSKRSSVR|SDAAMSR...	1.481
Q9GKY8	Rabbit	240	...ESKSSISSKRSSVR|SDAAMSR...	1.481

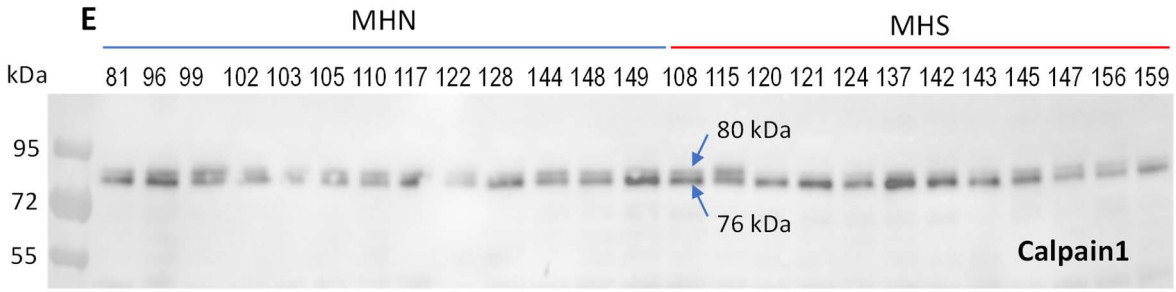

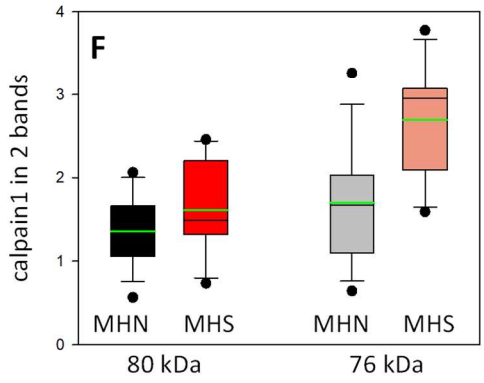

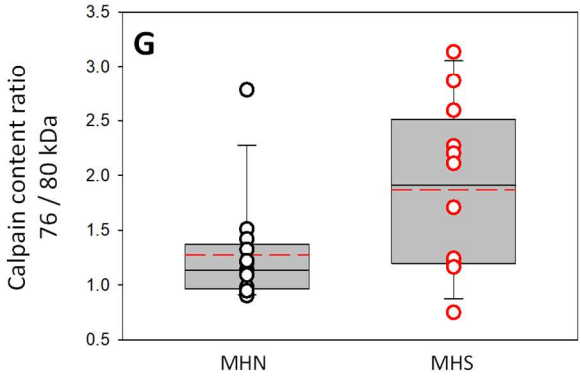

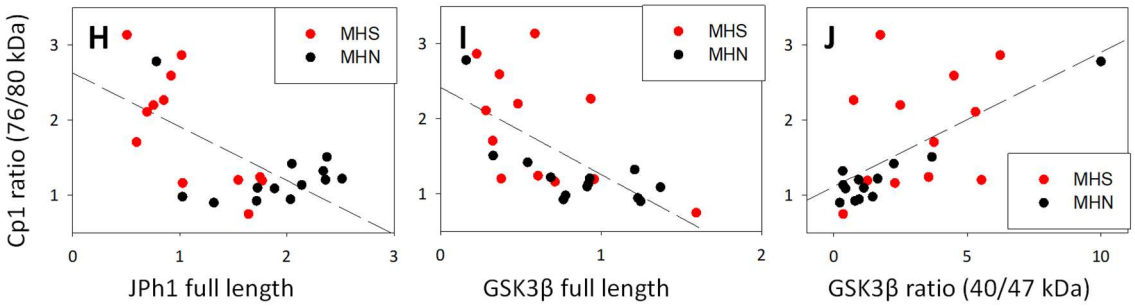

Figure 4. Activation and activity of calpain 1 in muscles of MHS patients. A, JPh1 sequence indicating conserved stretches and the two calpain cleavage sites with highest priority score, located between MORN motifs VI and VII. B, the 5 top-priority cleavage sites predicted by GPS-CCD 1.0 (36). C, JPh1 secondary structure, showing location of the highest priority cleavage site (R240-S241), helix-turn-helix DNA interaction site and TMD in SR junctional membrane. D, conservation of the preferred cleavage sites R240-S241 and S233-S234 in mammalian orthologs, which produce in every case a C-terminal fragment of ~ 44 kDa. E, WB of whole-tissue protein fraction in biopsied muscle of 13 MHN and 12 MHS patients, showing a dual band at ~80 kDa (details in expanded image Fig. 1 Supplement to Fig. 4). F, box plot of full-size and 76 kDa truncated forms, compared in the MHN and MHS groups. G, distribution of ratios of 76 /80 kDa forms. Median ratio in MHS (1.97) is 74% greater than that in MHN (1.13) with p = 0.029 of no difference. Automatic quantification of the WB is in Fig. 1 Supplement to Fig. 4. H, I, J, correlation of ratios of 76/80 kDa junctophilin 1 with contents of full-length JPh1 and GSK3β, and ratio of activated to full-length forms of GSK3β, derived by WB of the same muscle fractions used for the blot in panel E. The correlation coefficients R and p of no correlation are: for H, -0.65 and <0.001; for I, -064 and <0.001; for J, 0.61 and 0.001. Data trace. Panels E-G and H-J respectively in sections 6 and 5 of Calpain files with correlations ER IDL. JNB

The prediction tool GPS-CCD 1.0 (39) applied to JPh1 — the human sequence of which(40) is diagrammed in Fig. 4A — revealed several conserved calpain1 cleavage sites in multiple JPh1 orthologs (Fig. 4B). The one with highest score is at R240-S241, within the cytosolic domain, in-between MORN motifs 6 and 7 (Fig. 4A-C). In all these orthologs, cleavage at the R-S site will generate a C-terminal fragment of between 45.92 and 46.28 kDa, consistent with the ~44 kDa apparent size of JPh44.

To test the hypothesis that JPh1 is also cleaved by endogenous calpain1 in humans, we analyzed by Western blotting the calpain1 content of muscle from the patients with JPh content represented in Fig. 1. The immunoblot revealed a double band, with a component at ~80 kDa and another at ~76 kDa, consistent with the expected full-size and the autolysed activated fragment (Fig. 4E). We adapted a custom method to quantify immunoblots (22) to automatically compute the signal in closely placed double bands. Details of the procedure are in supplemental Fig. 1 to Fig. 4. Comparisons of the signal in the two bands between MHS and MHN patients are represented in Fig. 4F. The signal differences between MHS and MHN were not statistically significant for either calpain band. However, the paired ratios of band signals (76 kDa / 80 kDa, Fig. 4G) were on average > 50% higher in the MHS, with high statistical significance. This ratio, which can be taken as a measure of calpain activation, was negatively correlated with both the (full-size) JPh1 and GSK3β contents, and positively correlated with content of the 40 kDa GSK3β fragment, quantified in the same muscle samples (Fig. 4 H-J). The relative increase in the 76 kDa fragment was also accompanied by a higher content of smaller polypeptides detected by the calpain1 antibody (supplemental Fig. 2 to Fig. 4).

To test the ability of calpain1 to cleave human JPh1, total protein extracts from patients' muscle were incubated with 0.5 units of calpain1 at different time intervals (Fig. 5A, B). Incubation resulted in cleavage, as reflected in reduction in content of full-length JPh1 and increase of the JPh1 44-kDa fragment (still referred to as "JPh44", even though it was obtained by a different procedure). The changes were essentially completed in 5 minutes.

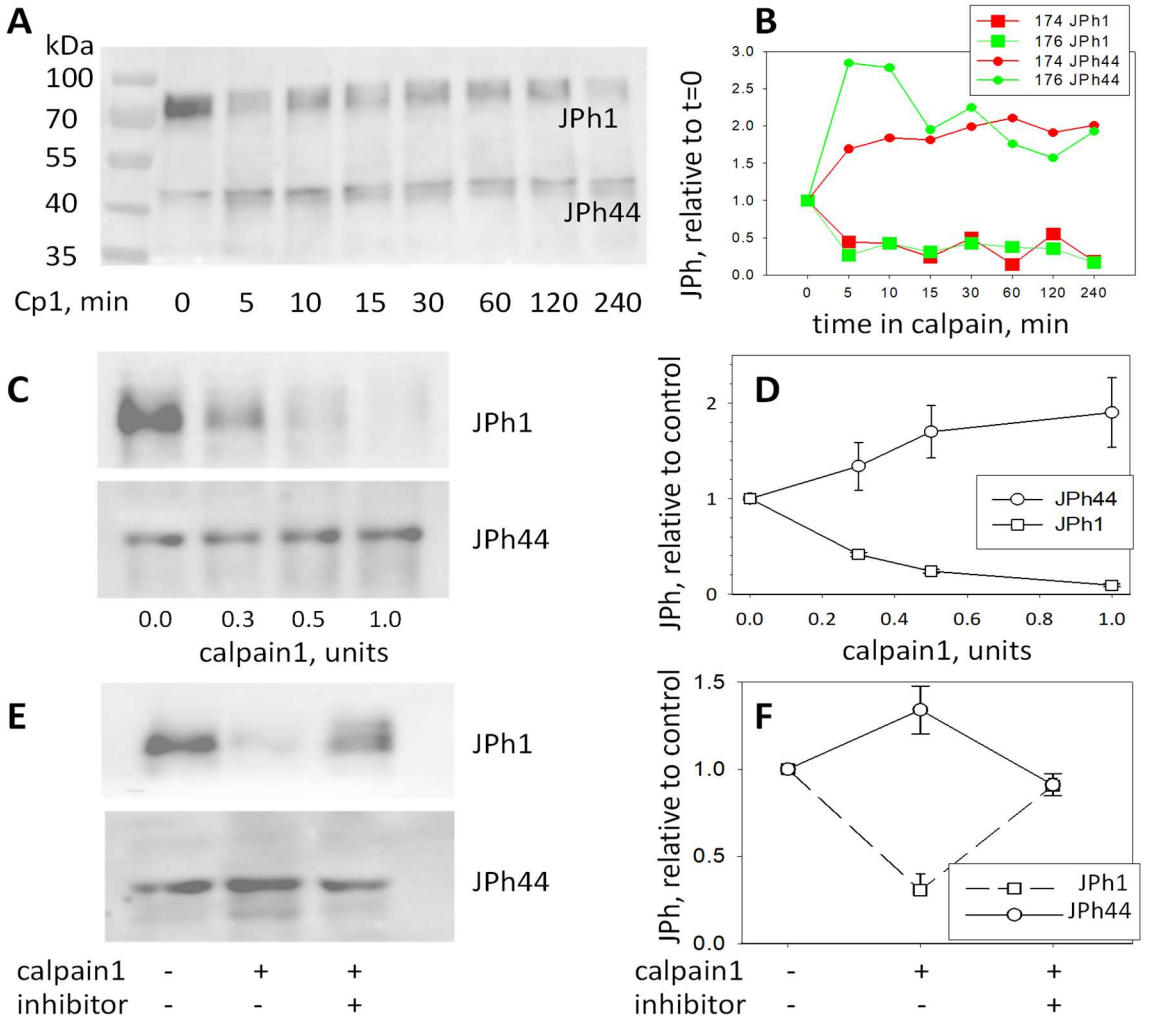
A
kDa
100
70
55
40
35
JPh1
JPh44
Cp1, min 0 5 10 15 30 60 120 240
B
174 JPh1
176 JPh1
174 JPh44
176 JPh44
JPh, relative to t=0
time in calpain, min
C
JPh1
JPh44
0.0 0.3 0.5 1.0
calpain1, units
D
JPh, relative to control
JPh44
JPh1
calpain1, units
E
JPh1
JPh44
calpain1 - + +
inhibitor - - +
F
JPh, relative to control
JPh1
JPh44
calpain1 - + +
inhibitor - - +

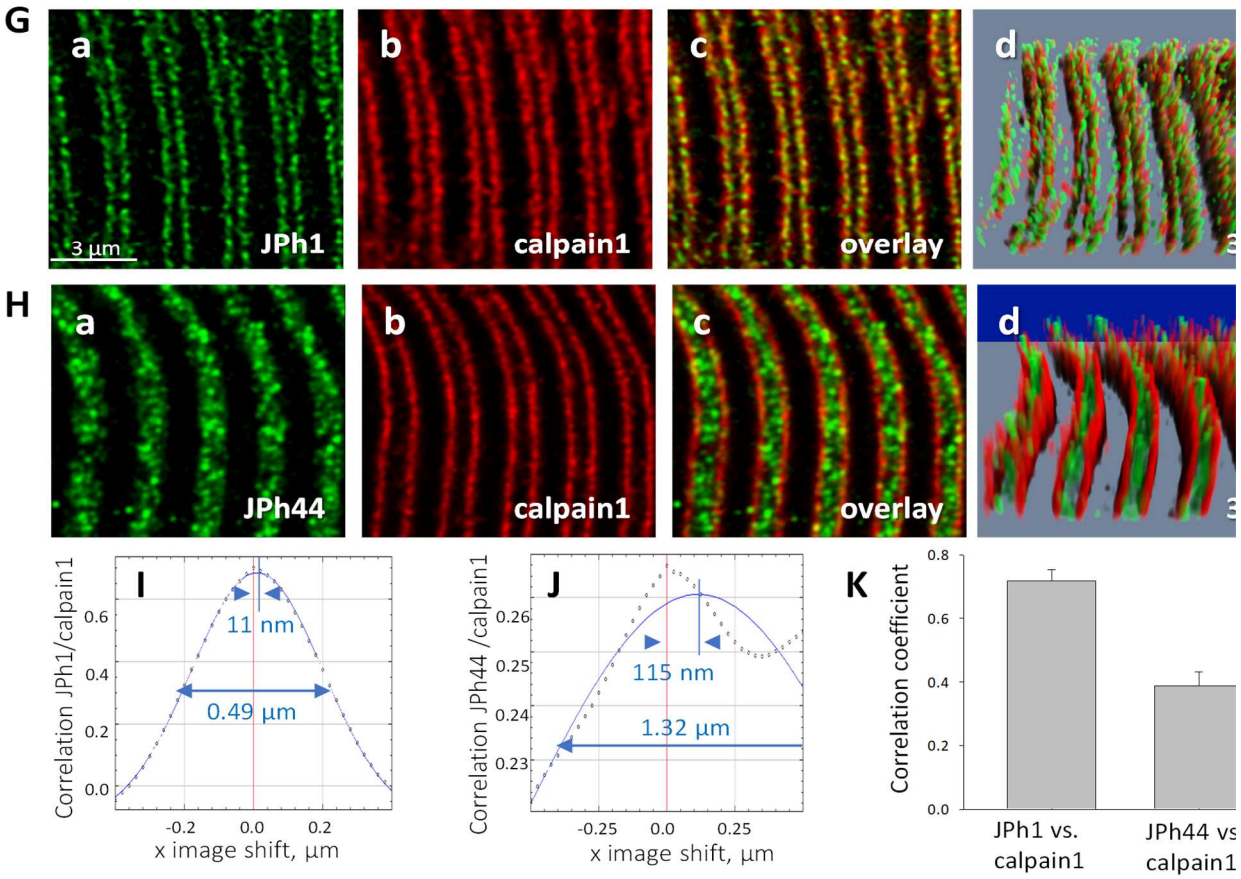
G
a
b
c
d
3 µm
JPh1
calpain1
overlay
H
a
b
c
d
JPh44
calpain1
overlay
I
Correlation JPh1/calpain1
11 nm
0.49 µm
x image shift, µm
J
Correlation JPh44 /calpain1
115 nm
1.32 µm
x image shift, µm
K
Correlation coefficient
JPh1 vs. calpain1
JPh44 vs calpain1

Figure 5. Calpain 1 effects and cellular location. A, B, time dependent changes in content of JPh1 and JPh44 in total protein extracts from patients' muscle, incubated with 0.5 units of calpain1 for different intervals. Quantities in B are normalized to initial value. Colors represent different experiments, on tissue from different individuals (2 replicates). C, D, effect of different concentrations of calpain1 incubated for 10 min with the same protein extract (n = 5 replicates in extracts from 5 different patient biopsies). Bars depict SEM. E, F, effect of calpain 1 at 0.5 units for 10 min, in the absence or presence of MDL28170 (n = 5 replicates). G, H, confocal images (individual slices of a z-stack, corrected for optical spread) of JPh1 (G) and fragment JPh44 (marked respectively with antibodies A and B), in muscle co-stained for calpain 1. Gd and Hd are 3D representations of the full z-stack of images showing movement of JPh44 away from T-SR junctions (labeled by calpain) and into the I band. I, J, Van Steensel's plots (Methods) show large difference in colocalization parameters VS shift and FWHM, quantifying movement of JPh44 away from calpain. K, pixel-by-pixel correlation between calpain and JPh1 or JPh44 signals. As shown by statistical analysis of replicates in Table 4, the differences in colocalization parameters are highly significant. Data trace. A, B, and E, F in Calpain files with correlations ER IDL.JNB (sections 1 and 4). G, H, experiment 081020a Series 5 and 081020b Series2, patient ID #183, MHS.

The effects on the two forms increased with calpain1 concentration, being again large and reciprocal (5C, D).

Finally, calpain-dependent JPh1 fragmentation was effectively inhibited in the presence of the calpain inhibitor MDL 28170 (Fig. 5E, F), an observation that strengthens the evidence of calpain1-specific cleavage of human JPh1.

While calpain1 is freely diffusible in the presence of normal cytosolic concentrations of Ca^{2+}, it binds to cellular structures immediately upon elevation of $[Ca^{2+}]_{cyto}$, which implies that its proteolytic activity can only be exerted on substrates that are close by at the time of activation (41,42). Therefore, to target JPh1 effectively, calpain1 must be present near T-SR junctions. To define this location precisely, human myofibers and human-derived primary myotubes were stained for calpain1, junctophilin (using antibodies A or B), and RyR1 as junction marker, and 3D-imaged at high resolution. Images of endogenous calpain1 in myofibers show that it colocalized with JPh1 (Fig. 5G) — confirming the presence of the protease near junctions — while JPh44 was found in the I band, not colocalized with calpain1 (5H). The quantitative measures described for colocalization of JPh and RyR1 were also indicative of colocalization of calpain1 with JPh1, but not with JPh44 (Fig. 5 I-K and Table 3).

Effects of exogenous calpain on living cells

The effects were studied by heterologous expression of tagged calpain1 in patient-derived myotubes and by extracellular perfusion of human and C2C12 myotubes. The main effect of the overexpressed calpain1 was an increase in intranuclear localization of JPh (Table 4), illustrated in Fig. 6 with images of a human-derived culture transfected with FLAG-calpain1. Panels 6A-D are 3D renderings of the z-stacks of confocal images. A and B show FLAG-calpain1 and junctophilin (stained with antibody A, which in myotubes marks both JPh1 and JPh44). Panel C renders RyR1 in the same cells. The images allow direct comparison, within the same field, of a myotube (Cell 1) that expressed strongly the FLAG-tagged calpain1, and one (Cell 2) that had no trace of the protein. Calpain1 (panel A) was widely distributed in the cytosol; nuclei can be recognized in A and C by the absence of calpain1 and RyR1. While JPh (panel B) was widely distributed in Cell 2, in Cell 1 it resided mostly inside nuclei, presumably because it consisted largely of JPh44, cleaved by the excess calpain. The intranuclear junctophilin in Cell 1 adopted a diffuse, fine-grained form, while the cytosolic junctophilin in Cell 2 often formed puncta or clusters. The increase in nuclear location of junctophilin in cells expressing calpain was large and highly significant (Table 5).

RyR1 is clustered in both cells (Fig. 6C, G). The overlay (D) shows that junctophilin colocalizes with RyR1 (red) in Cell 2, where it should be largely in JPh1 full-size form, but not in calpain-expressing Cell 1, where it is largely

inside nuclei, presumably as the JPh44 fragment. Colocalization of JPh and RyR1 was stronger in cells not transfected with FLAG-calpain1, with highly significant differences in all 4 measures (Table 5).

Panels 6E-G show fluorescence in one slice of the z-stack, with pairwise overlays in H-J. The calpain1-rich cytosol of Cell 1 shows JPh1 in particulate form, without clusters (Panel H). The same region shows abundant clusters of RyR1 (6G, I). Cell 2, which lacks exogenous calpain1, shows abundant JPh1 in clusters (F), in almost perfect colocalization with RyR1 (J), which identifies these puncta as JPh1 in developing T-SR junctions. In Cell 1, where calpain1 was expressed, the protease was also clustered (panel E), highly colocalized with RyR1, i.e., located at T-SR junctions (panel 6I, colocalization quantified in Table 7). As argued by Murphy (42), the location of calpain1 at calcium release sites is consistent with the idea that Ca^{2+} activation of calpain1 causes its binding to structures, an effect that positions the protease ideally for cleaving JPh1.

Fig. 6 illustrates an additional, frequent observation that we did not pursue further: the cell that expressed the calpain construct (Cell 1) had much greater density of RyR1, consistent with other evidence of a role of the protease in control and promotion of muscle development (e.g. (43)).

Similar effects were observed upon exposure of cells to extracellular calpain1. Based on evidence that calpain1 can permeate cell membranes (44), we incubated patient-derived myotubes as well as differentiated C2C12 line cultures with calpain1 or vehicle (5 µg/ml or 45 nM) for 24 hours. Fig. 7 illustrates the effects on the distribution of JPh. In human myotubes, calpain treatment resulted in an increase in junctophilin inside nuclei (7Ab vs. Bb, Table 7). It also reduced its colocalization with RyR1 in cytosolic clusters, which is high in untreated cells (7Ad vs. Bd, quantified in graphs 7K-N and Table 8). In C2C12 cells, the treatment resulted in a lower density of JPh in the cytosol, with increase inside nuclei (7Cb, Table 9), presumably of the JPh44 fragment. These were C2C12 myotubes transiently expressing JPh1 with the Myc tag at its N terminus (a gift from Prof. V. Sorrentino); as JPh44 moved into nuclei in the calpain-treated muscles (7Cb), the Myc tag remained outside nuclei (7Cc), an observation that strengthens the conclusion that JPh44 is a C-terminal cleavage fragment.

Together, the results are consistent with calpain1 activation and autolysis in MHS patients by virtue of their elevated $[Ca^{2+}]_{cyto}$, accompanied by localization of the protease at T-SR junctions, where it cleaves JPh1 to produce JPh44. The activated calpain1 also produces the 40 kDa, activated form of GSK3β.

Figure 6. Effect of heterologous expression of calpain 1 on patient-derived myotubes. A-D, 3D rendering of a z-stack of confocal images from a culture of primary myotubes transfected with FLAG-calpain 1 (panel A), co-stained for junctophilin 1 (with antibody A, staining both JPh1 and JPh44, panel B) and RyR1 (panel C). While one of the myotubes (Cell 1) expresses calpain 1 abundantly, the other (Cell 2) does not. In Cell 1, junctophilin adopts a fine-grained appearance and occupies nuclei (e.g., ellipse in B), recognizable by the absence of RyR1 (C, D). In Cell 2 junctophilin is distributed in the cytoplasm, partly colocalized with RyR1. Statistics of nuclear vs. cytosolic location, comparing cultures with and without calpain, are in Table 5. E-G, an individual x-y image (slice) in the z-stack, with sub-sections magnified and superimposed to illustrate colocalization. H, calpain colocalizes poorly with junctophilin in Cell 1, as junctophilin is largely in cleaved, JPh44 form. I, calpain colocalizes highly with RyR1, forming clusters. J, in Cell 2, which does not express calpain, junctophilin colocalizes highly with RyR1, presumably as full-size JPh1. K-N, Van Steensel's and Li's plots, showing poor colocalization of junctophilin and RyR1 in Cell 1 (K,L), contrasting with that in Cell 2 (M,N). Statistics of colocalization measures, comparing cultures with and without calpain, are in Table 6. Data trace. Experiment 073020La Series 5. Myotubes derived from patient #180, tested as MHN. Data in *ColocalizJp44andRyR.JNB* sections 5 and 11.

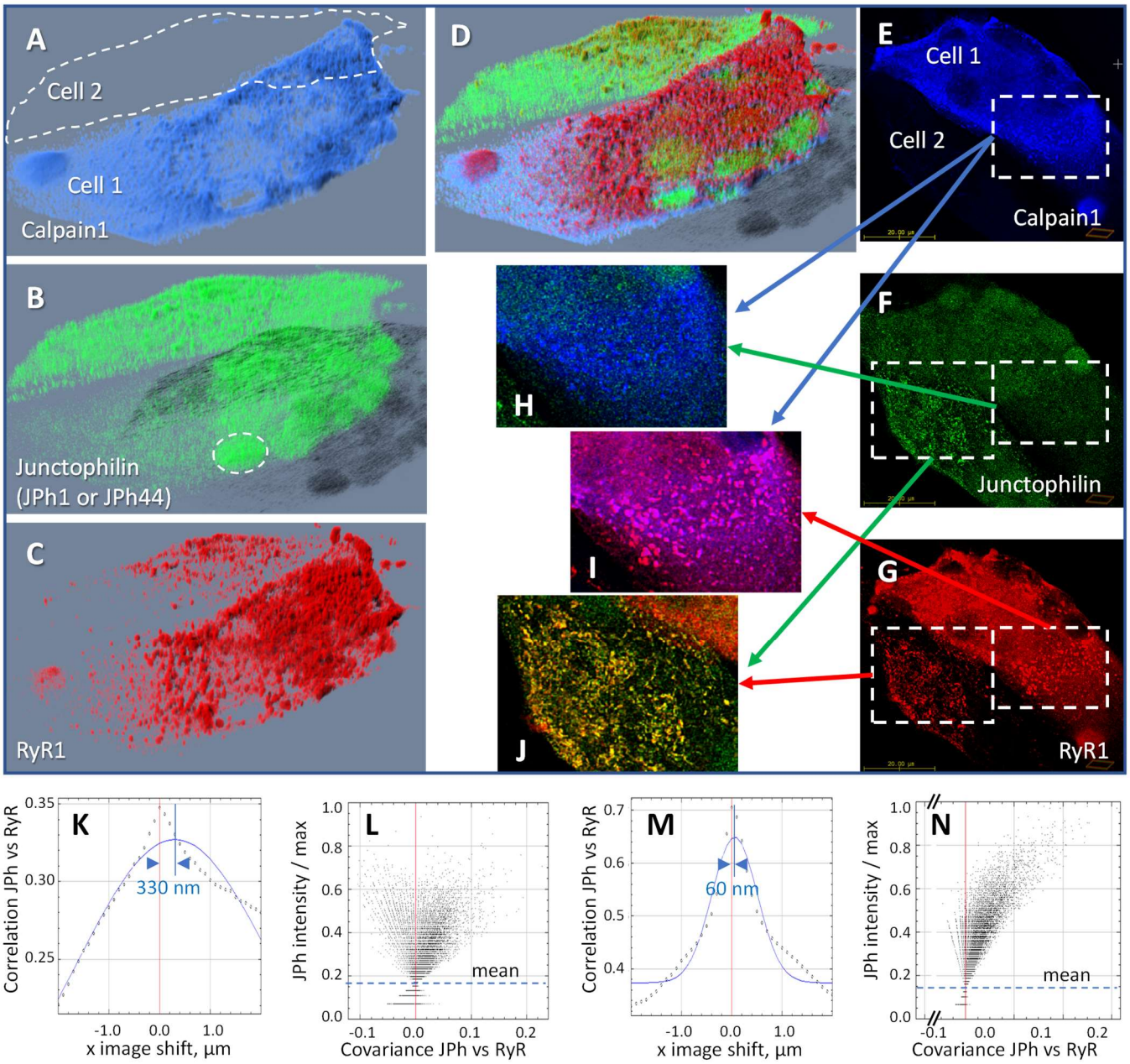

Effects of a JPh1 deletion mutant in mouse muscle and a muscle cell line

The presence of the JPh44 fragment in the nucleus suggested that it might play a role in gene transcription. The calpain algorithm locates the likely cleavage site at between R240 and S241. To test the prediction and produce a probe of the roles of the JPh44 fragment, we generated the plasmid GFP-Δ(1-240) JPh1, coding for the N-terminal fusion of GFP with the human JPh1 deletion variant that starts at S241, and studied its expression in FDB muscles of adult mice, transfected by electroporation. Panels A and B in Fig. 8 compare expression of GFP-JPh1, the full plasmid, with the GFP-tagged deletion variant (GFP-Δ(1-240) JPh1) in myofibers co-stained for RyR1. While the full-size protein remained near RyRs, in triad junctions, the deletion variant moved away, into the I band, in a manner reminiscent of the movement of JPh44 (compare with Fig. 2 A, B). The movement away from triads (marked by RyR1) was quantified by colocalization metrics (Table 10 and supplemental Fig. 1 to Fig. 8). Panels 8C and D demonstrate intra-nuclear localization of the deletion variant, reaching concentrations that saturate the light detector at the excitation intensities required to reveal the sarcomeric expression of the protein (e.g., 8C).

The similarity of movements and cellular location between the native JPh44 and the exogenous deletion mutant are consistent with a tentative identification of JPh44 as the C-terminal piece of JPh1 with N terminus at S241. The sole alternative sequence consistent with the predictive algorithm, starting at S234, would only differ for having 7 additional residues at the N terminus. Based on this likely identification, we used GFP-Δ(1-240) JPh1 as stand-in, to uncover the effects of the native JPh44 fragment on gene transcription and translation.

GFP-Δ(1-240) JPh1 was transfected into C2C12 cells, which expressed it well, showing abundant GFP content inside nuclei (Fig. 9A). Gene expression analysis revealed that 121 and 39 genes were respectively repressed or induced ($P < 0.01$) in the transfected myoblasts, compared with control cells (Fig. 9B). KEGG pathway-enrichment analysis identified these genes as intimately related to multiple processes, including regulation of the PI3K-Akt-glucose signaling pathway, energy metabolism, muscle growth, and lipid metabolism (9C). Specifically, GSK3β and other genes such as Pck1 (phosphoenolpyruvate carboxykinase 1), RBP4 (retinol-binding protein 4), APOC3 (apolipoprotein C3) and TRAF3 (TNF receptor-associated factor 3), which are inhibitory of phosphorylation of Akt/protein kinase B, were inhibited in response to expression of the construct.

As expected from the observed effects on transcription, we found by Western blot analysis a reduction in GSK3β content in cells transfected with GFP-Δ(1-240) JPh1, by 40% of the content in cells expressing GFP alone (Fig. 9D). The difference was statistically significant (Fig. 9E). By high-resolution imaging we found that cells expressing the JPh deletion construct had reduced levels of GSK3β when compared to the neighboring non transfected cells (Fig. 9G, H and Table 11) whereas cells expressing the vector coding for GFP and otherwise empty had similar GSK3β levels to its neighboring cells (Fig. 9F and Table 11).

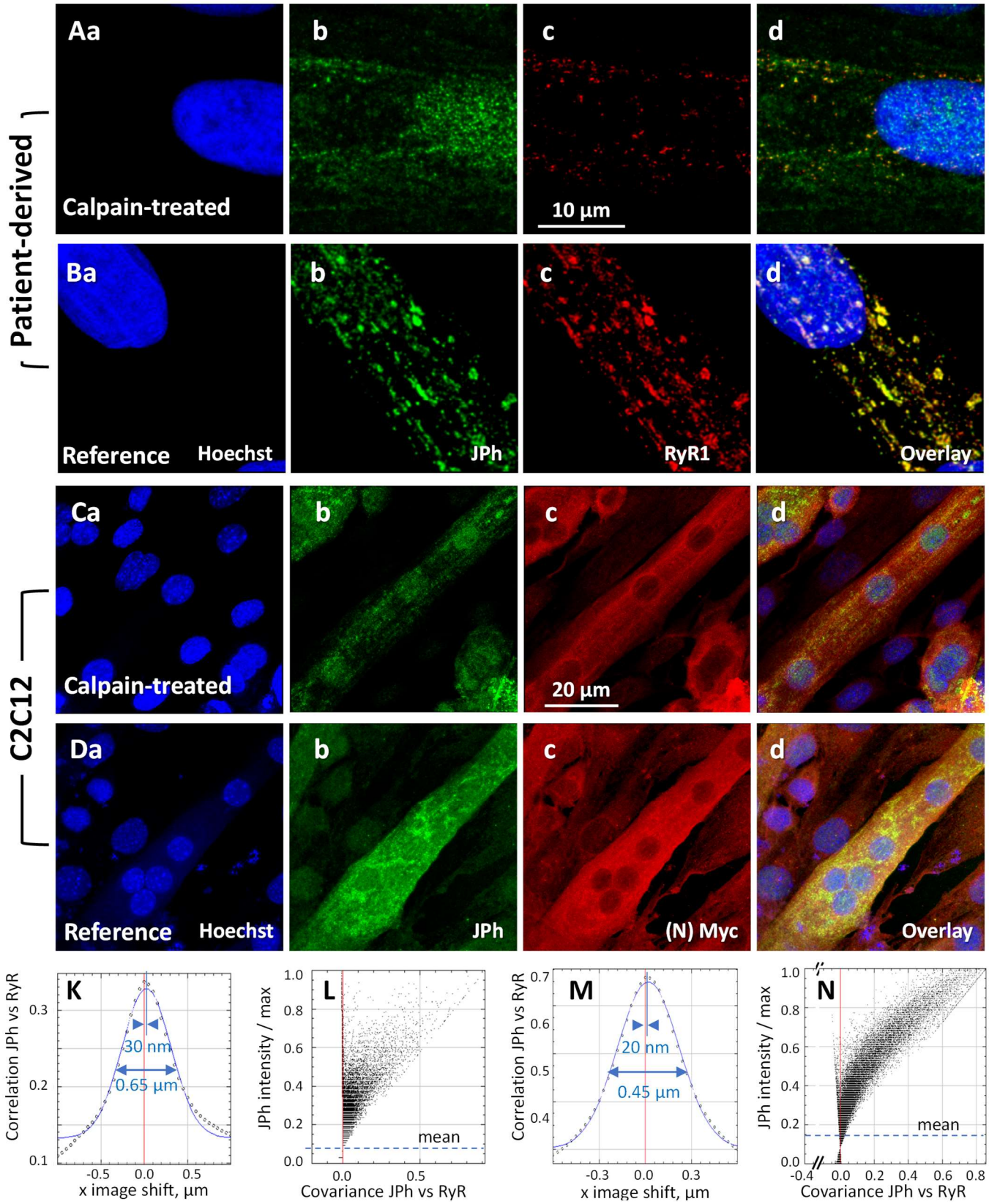

Figure 7. Effects of extracellular perfusion with calpain 1. A-D, high-resolution confocal images of patient-derived (A, B) or differentiated C2C12 myotubes (C, D) exposed to calpain1 (5 µg/ml or 45 nM) or vehicle for 24 hours. Cells. In human myotubes co-stained for junctophilin (antibody A) and RyR1, calpain exposure increased junctophilin inside nuclei (Ab vs. Bb, Table 8) and reduced its colocalization with RyR1 in cytosolic clusters (Ad vs. Bd and Table 9). In C2C12 cells (transiently expressing (N)Myc-JPh1 stained with antibody A) calpain lowered junctophilin density in the cytosol, and increased it inside nuclei (Cb, Table 9). The Myc tag remained outside nuclei (7Cc). K-N, the loss of colocalization of junctophilin and RyR in human myotubes was quantified by the increase in VS shift and FWHM (compare K – calpain-treated – and M –reference), and

the characteristic features of Li's plot (L – treated – vs. N – reference). The changes were significant, as shown by replication statistics in Table 9. Data trace. Human-derived primary myotubes. Patient #173 030320a series 5 (reference) and 030320b series 10 (calpain treated). C2C12 myotubes. 032720a, series 1 (treated) and 032720b, series 5 (reference). Nuclear localization data in in Calpain files with correlations ER IDL.Jnb Section 9 (Calpain treatment of human muscle). Colocalization data in ColocalizJP44 and RyR.JNB Section 9. #180 MHN.

Discussion

Starting from the observation of reciprocal differences in content of the structural protein JPh1 and its fragment JPh44 in muscle of patients with chronically elevated cytosolic Ca^{2+}, we here identified the pathogenic mechanism leading to these differences. We also demonstrated gene regulatory roles of JPh44. These regulations turned out to be largely compensatory of the pathogenic consequences of the elevated $[Ca^{2+}]_{cyto}$.

Junctophilin 1, calpain 1 and the kinase of glycogen synthase undergo fragmentation in MHS patients

Junctophilin(5) is one of the 5 proteins deemed essential for functional, skeletal muscle-style calcium signaling for EC coupling. We now show that the 72 kDa full-size protein is reduced by ~50% in total protein extracts of muscles of MHS patients (Fig. 1A, C). A 44 kDa fragment increased in the same patients, albeit in a lesser proportion, a discrepancy that we take as evidence of production of other fragments (Fig. 1B, D, E).

These changes join a wide-ranging pathogenic alteration of cellular metabolism in these patients, which comprises changes in content, distribution and posttranslational modification of multiple proteins. The observed modification of multiple molecular players of glucose utilization by muscle is the likely cause of the hyperglycemia and diabetes that disproportionally affects MHS patients (22,23). Here we demonstrate an increase in the cleavage of GSK3β from the original ~47 kDa molecule to a ~40 kDa form, a truncation that activates the enzyme (29–31). Muscle-specific ablation of this protein inhibits glycogen synthase in mice, improving glucose tolerance correlated with enhanced insulin-stimulated glycogen synthase activation and glycogen deposition (45). Therefore, we surmise that the activation of GSK3β found in these patients constitutes an additional link in the pathogenic chain that leads from increased $[Ca^{2+}]_{cyto}$ to alteration in muscle utilization of glucose, then to hyperglycemia and diabetes (22,23,46).

The present study used techniques for imaging protein localization that, as documented in our recent work (22), reached a spatial resolution beyond the theoretical optical limit, unprecedented in studies of live muscle. From this vantage point, we demonstrate the consequences of cleavage of junctophilin1. The full-size molecule is located at T-SR junctions (as demonstrated by quantitative measures of colocalization with RyR1; Fig. 2 A, C, and Table 1). In contrast, the fragment JPh44 leaves the junctions and migrates largely into the I band, presumably via non-junctional SR (Fig. 2B, C, and Table1).

The fate of JPh44 was further followed on primary myotubes derived from patients' muscle, where it was seen to migrate inside nuclei (Fig. 2E, F). By contrast, JPh1 remained outside nuclei, largely in clusters, in all likelihood corresponding to developing T-SR junctions, as revealed by high colocalization with RyR1 (Fig. 2Dd, Fa, b and Table 1).

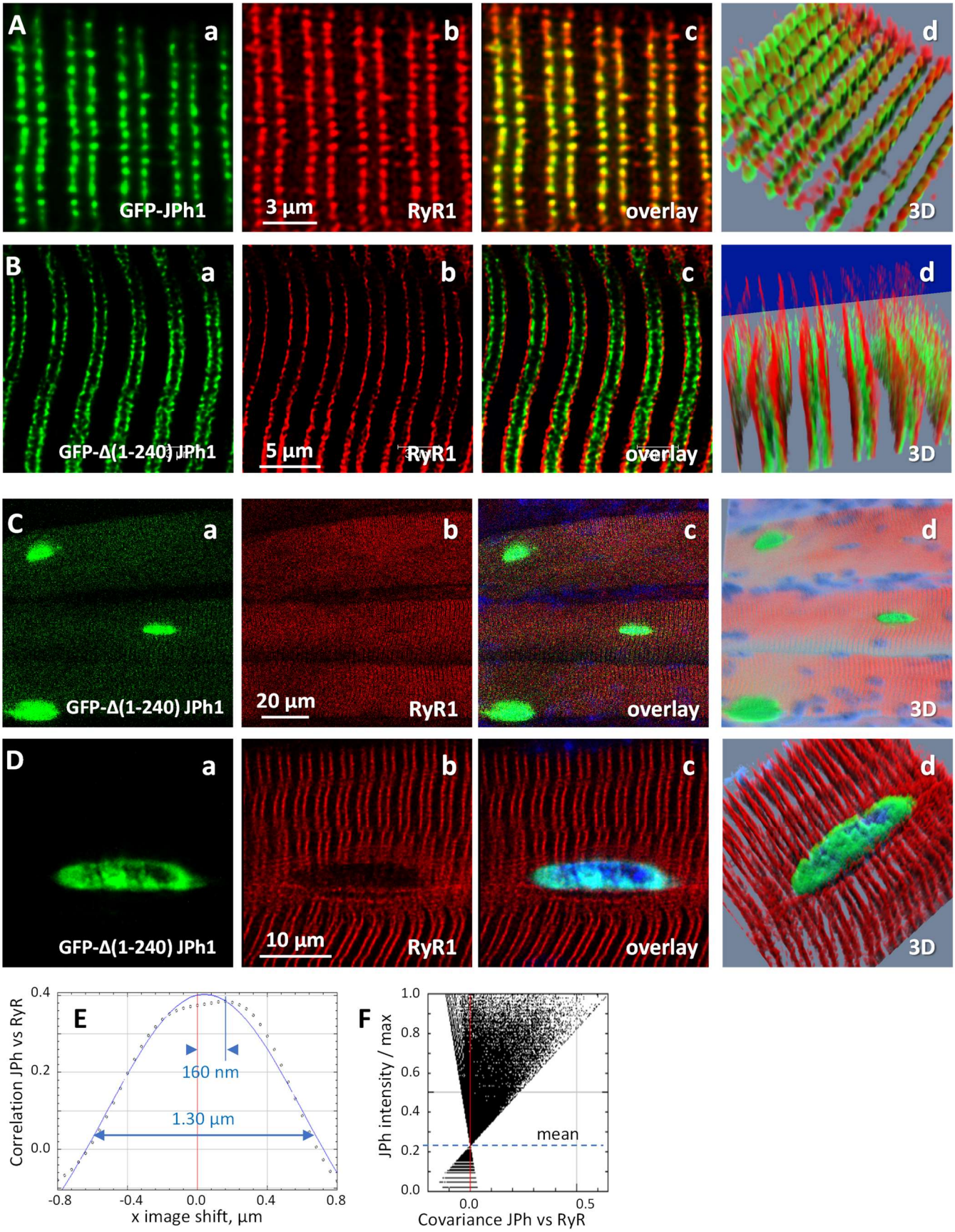

Figure 8. Expression of GFP-Δ(1-240) JPH1 and GFP-JPh1 in adult mouse muscle. A, confocal images of mouse FDB myofibers electroporated with plasmids encoding GFP-tagged, full-length JPh1, co-stained for RyR1. B, mouse FDB myofibers electroporated with plasmids encoding GFP-Δ(1-240) JPh1. C, D, demonstrate the nuclear distribution of the protein upon

electroporation of GFP-JPh1 Δ1-240. E, F, Van Steensel and Li plots, showing absence of colocalization between the exogenous construct and RyR1. Statistics of colocalization measures are in Table 12. Data trace. Source files: A, experiment 111220Lb, Series 1. B-D, 110920La, Series 1, 8, 9.

To define the primary sequence of JPh44, the construct (N)GFP-JPh1-FLAG(C) was expressed in myotubes and adult mouse muscle. The consistent presence of the FLAG tag inside nuclei (illustrated in Fig. 3A-C and quantified in Table 2) plus the persistence of the N-terminal GFP in the cytosol, forming clusters analogous to those of JPh1 and RyR1 (Fig. 2) in myotubes and staying aligned with junctional triads in myofibers (Fig. 3C) unambiguously indicate that the JPh44 fragment includes the C terminus of JPh1. The persistence of GFP outside nuclei indicates that the N-terminal fragment cleaved from JPh1 conserves at least some of the MORN motifs by which JPh1 attaches to T tubule and plasma membranes (7). However, the stable location of the N-terminal cleavage fragment of JPh1 at triad junctions is inconsistent with the proposal that assigns the specific triadic location of JPh1 to its ability to dimerize (7), as this ability is likely lost in the N-terminal cleavage fragment.

In primary myotubes from human muscle expressing the construct, junctophilin increased inside nuclei (Fig. 7Ab, compare with Bb; statistics in Table 7), correspondingly reducing its clustering with extra-nuclear RyR1 (7Ad vs. Bd, quantified in graphs 7K-N and Table 8). Similar effects were observed in C2C12 cells expressing (N) Myc-JPh1 (7Cb, Table 9). The continued presence of the Myc tag outside nuclei in the calpain-exposed muscles (7C) confirms that JPh44 is a C-terminal fragment.

$[Ca^{2+}]_{cyto}$ determines JPh1 fragmentation and relocation

Direct perfusion of permeabilized human myofiber bundles with elevated Ca^{2+} concentrations resulted in reciprocal changes in JPh1 and JPh44 content (Fig. 3D-F). While the application of Ca^{2+} was only transient, the major, statistically significant changes that resulted are consistent with a causative involvement of the chronically elevated $[Ca^{2+}]_{cyto}$ in the pathogenic process that takes place in MHS muscle. This was accompanied by a large increase in JPh44 content in blots of the nuclear fraction extracted from MHS patients muscle (Fig. 3G, H) that positively correlated with the $[Ca^{2+}]_{cyto}$ measured in myotubes derived from the same patients (Fig. 3I). This correlation linked a feature of adult muscle with a measure in the derived culture, and notably also applied to JPh localization in patients' myotubes relative to their $[Ca^{2+}]_{cyto}$ values (Fig. 3J).

Probable identification of the cleavage site in junctophilin1

The identification of elevated $[Ca^{2+}]_{cyto}$ as mediator of the MHS cellular phenotype pointed at the Ca^{2+}-activated calpains as enzymatic agents of JPh proteolysis. An algorithm predictive of calpain cleavage sites within protein sequences (39) contributed evidence of involvement of calpain1. Among the predicted cleavage sites in JPh1, two had high priority scores (Fig. 4B). The one with the highest score, at R240-S241, is highly conserved in mammals (Fig. 4C), producing in every ortholog a C-terminal fragment of approximately 46 kDa. This exercise identifies JPh44 as the C-terminal fragment of JPh1 with N terminus at S241. The cleavage site S233-S234, also of high probability score, provides an alternative sequence, identical except for 7 additional aminoacid residues at the N

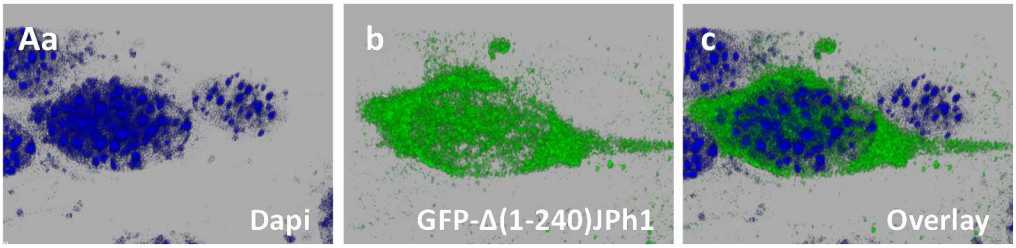
Aa
Dapi
b
GFP-Δ(1-240)JPh1
c
Overlay

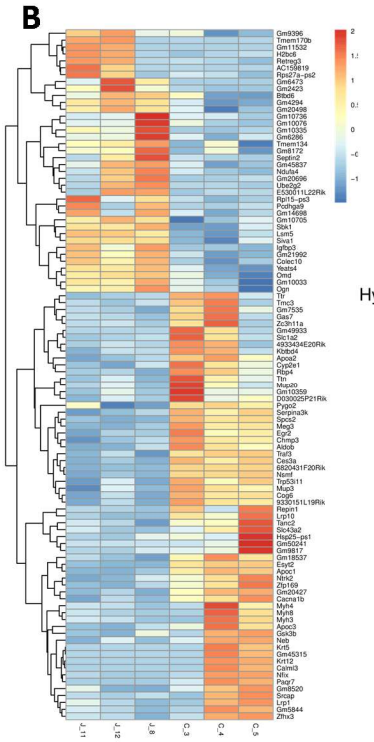
B

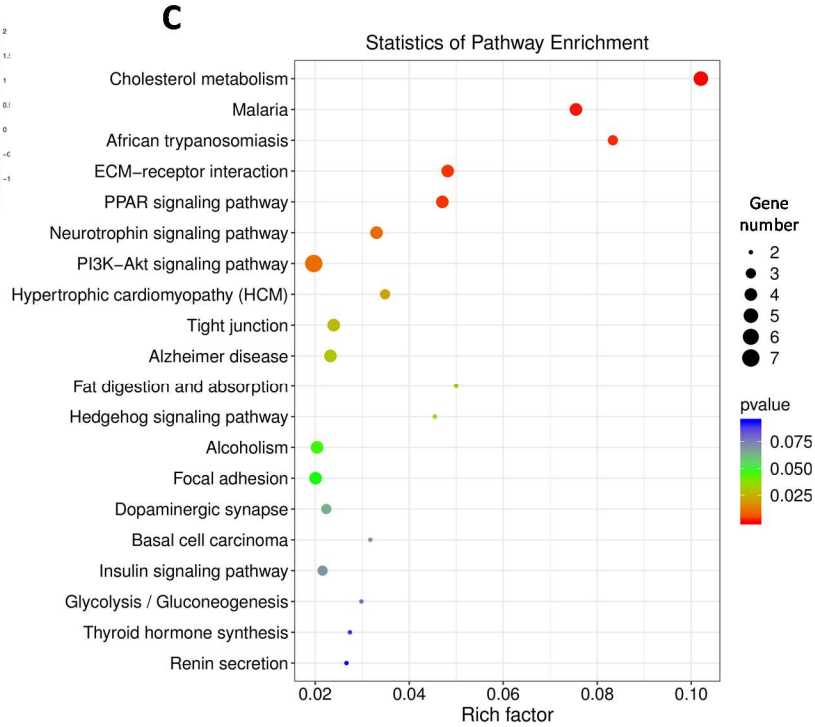
C
Statistics of Pathway Enrichment
Cholesterol metabolism
Malaria
African trypanosomiasis
ECM−receptor interaction
PPAR signaling pathway
Neurotrophin signaling pathway
PI3K−Akt signaling pathway
Hypertrophic cardiomyopathy (HCM)
Tight junction
Alzheimer disease
Fat digestion and absorption
Hedgehog signaling pathway
Alcoholism
Focal adhesion
Dopaminergic synapse
Basal cell carcinoma
Insulin signaling pathway
Glycolysis / Gluconeogenesis
Thyroid hormone synthesis
Renin secretion
0.02
0.04
0.06
0.08
0.10
Rich factor
Gene number
2
3
4
5
6
7
pvalue
0.075
0.050
0.025

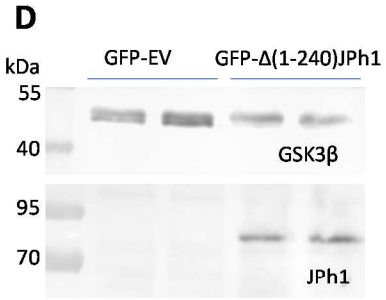
D
kDa
GFP-EV
GFP-Δ(1-240)JPh1
55
40
GSK3β
95
70
JPh1

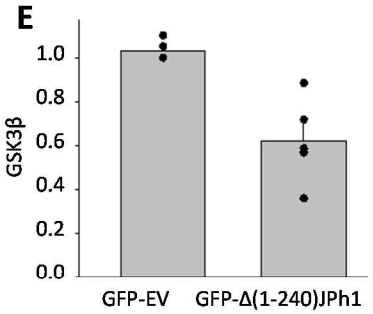
E
GSK3β
1.0
0.8
0.6
0.4
0.2
0.0
GFP-EV
GFP-Δ(1-240)JPh1

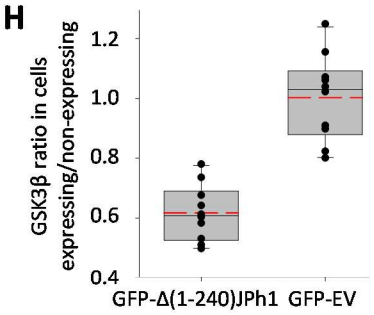
H
GSK3β ratio in cells expressing/non-expressing
1.2
1.0
0.8
0.6
0.4
GFP-Δ(1-240)JPh1
GFP-EV

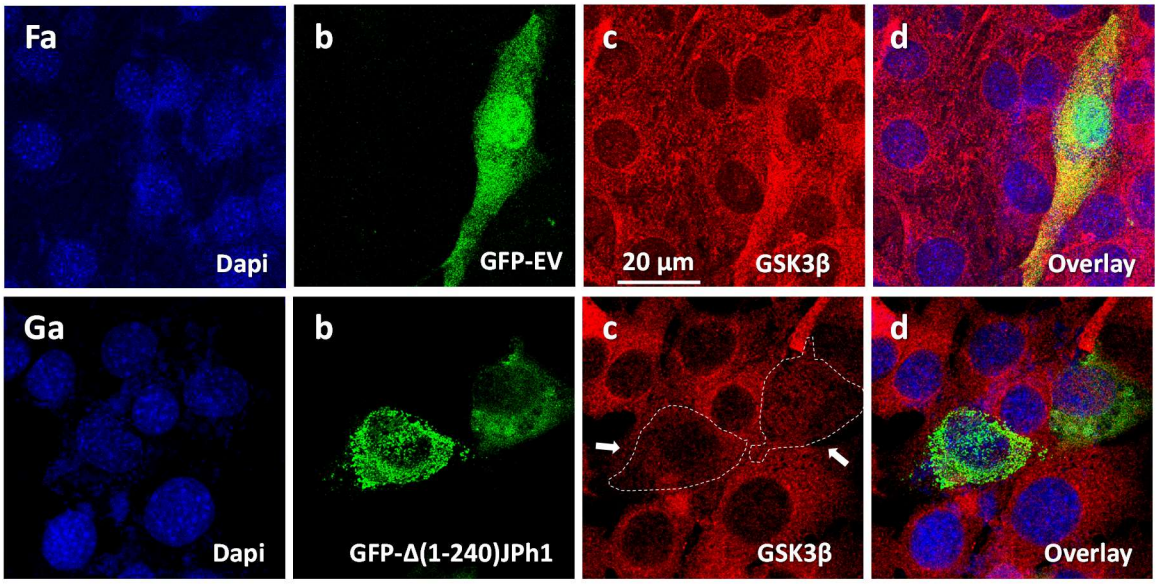
Fa
Dapi
b
GFP-EV
c
20 μm
GSK3β
d
Overlay
Ga
Dapi
b
GFP-Δ(1-240)JPh1
c
GSK3β
d
Overlay

Figure 9. Regulation of transcription in C2C12 myoblasts. A, confocal images of C2C12 cells transfected with GFP-Δ(1-240) JPh1 vector, showing the expressed protein inside nucleus. B, heat map of significantly altered genes in C2C12 myoblasts expressing GFP-empty vector or GFP-Δ(1-240) JPh1. C, KEGG pathway enrichment analysis of transcripts significantly altered by GFP-Δ(1-240) JPh1. D, Western blot of GSK3β in total cell extracts from C2C12 cells expressing GFP-empty vector or GFP-Δ(1-240) JPh1. E, GSK3β protein signal in WB of panel D. F, confocal image of GSk3β immunofluorescence (red), in C2C12 cells transfected with GFP-empty vector, to compare cells that expressed the marker (green) with those that did not. G, image for similar comparison of GSK3β content in culture transfected with GFP-Δ(1-240) JPh1, showing deficit of GSK3β in expressing cells (green). Statistics of replications in Table 13 shows high significance of the difference. Data trace. Source files: A, experiment 110121La series 003. B, C, gene expression profiling data in Dropbox / JPh / manuscript / Figure 9 panels. D, uncropped blots and normalizing gels in raw western blots and original gels.doc. E, in GSK3Blevels.JNB in Dropbox / JPh / manuscript / Figure 9 panels. F, experiment 102921La series 009. G, 110321 Lb series 007. H, GSK3B graphs and statistics.JNB, section 4. In Manuscript\Figure 1.

terminus. The extra residues would neither cause a difference in molecular weight detectable by electrophoresis nor would be expected to change other physicochemical properties, including putative gene regulatory functions suggested by the nuclear localization. Both cleavage sites predict an N-terminal fragment that contains 6 MORN motifs, a prediction consistent with the observation that the N-terminal fragment of JPh1 stays at T-SR junctions (Fig. 3).

A key finding of this study is the discovery of a link between elevated $[Ca^{2+}]_{cyto}$ and activation of calpain to directly cleave JPh1. Activation occurs in a relatively narrow range of elevated $[Ca^{2+}]$ (50-300 nM) and includes autolysis of its main subunit, which removes an N-terminal piece to bring the molecular weight from 80 to 76 kDa (36–38). We found the fraction of calpain1 in 76 kDa form in MHS muscle significantly higher (by ~80%) than in controls (Fig. 4D, F). The implication that this piece represents activated protease was affirmed by the high negative correlation between the drop in JPh1 content and the fraction of truncated protease in MHS muscle (Fig. 4G). A negative correlation of similar significance with content of the full length GSK3β evinces an additional role of calpain1, proteolysis and activation the kinase (Fig. 4H, I).

In agreement with the predictive algorithm, calpain1 cleaved the JPh1 protein extracted from human muscle *in vitro,* in a time- and concentration-dependent manner, to a form with the same apparent molecular weight of the native fragment we call JPh44, an action suppressed by a calpain inhibitor (Fig. 5).

Additional evidence linking calpain activation to JPh1 cleavage was obtained by applying calpain directly to living cell preparations. As illustrated in Fig. 6, heterologous expressed calpain caused a visible increase of JPh44 — distinct from the full-size protein for adopting a fine-grained appearance— which moved massively into nuclei (seen in Cell 1 of panels 6B and D and supported by quantification in multiple cells, Table 4). Concomitantly, the colocalization of JPh and RyR1 was diminished (Table 5). Also consistent with cleavage of JPh1 by the heterologous calpain1 is the high colocalization of the two molecules, contrasting with the low colocalization of JPh44 and the protease (Table 3).

Previous studies reported that calpains cleave couplon proteins, including RyR1 (47) and STAC3 (48). The present findings show that the protease is at the right location for those actions. Both endogenous calpain1, imaged by immunofluorescence in human muscle (Fig. 5G), and FLAG-tagged calpain1 (Fig. 6I) were found precisely located at triad junctions; the location was confirmed by its high colocalization scores with JPh1 and with RyR1 (statistics

in Tables 3 and 6). The observations support the proposal of Murphy et al. (37) that the protease is freely diffusible in apo form but binds to cellular structures immediately upon exposure to high [Ca^{2+}]. Indeed, the quantitative measures of colocalization with RyR1, especially the spatial shift and Gaussian spread obtained with the Van Steensel method, show that the junctional protein JPh1 has a tighter overlap with RyR1 than calpain1 (Table 6), which suggests the coexistence of bound and diffusible forms of the protease.

From Ca^{2+} dysregulation to hyperglycemia and diabetes

The results reviewed above establish with a high degree of confidence that the reduction in JPh1 content observed in MHS patients is caused by calpain1 activated by excess cytosolic calcium and that the activated calpain also cleaves the specific kinase of glycogen synthase GSK3β, with inhibitory consequences on glycogen synthesis. This effect, together with the putative cleavage of the regulated glucose transporter GLUT4 (49), impair glucose utilization by muscle.

In 2019, Altamirano et al. (23) first called attention to the high incidence of hyperglycemia and diabetes, developing in patients years after they were diagnosed with MHS. Aware that the main proximate cause of insulin resistance and hyperglycemia is failure of glucose processing by muscle (e.g., (46)), we set out to understand the pathogenic pathway linking MHS and diabetes. The question is relevant beyond the MHS syndrome, as a similar dysregulation of Ca^{2+} homeostasis is found in other conditions, including related inheritable diseases with mutations in couplon proteins (9,50,51), DMD (17–19), Exertional and Non-exertional Heat Stroke (52,53) and Statin-related Myotoxicity (54). We found a wide-ranging alteration of location and phosphorylation of the enzymes that manage storage of glucose as glycogen in muscle, namely glycogen synthase, glycogen phosphorylase and their controlling kinase PhK (55), leading to a shift of the glucose ←→glycogen balance towards glycogenolysis(22). Additionally, we found a decrease in the deployment (translocation) of GLUT4 (22).

The present study adds two nested mechanisms that operate in the same direction: first, the activation by Ca^{2+} and autolysis of calpain1 (Fig. 4D-F). Because calpain1 is known to lyse GLUT4 and increase its turnover (49), its activation is a likely explanation for the observed decrease in translocation of the transporter (22). The second link to diabetes is the observed activation, again by proteolysis mediated by the activated calpain, of GSK3β (documented with Figs. 1F-I and 4H, I). The activated kinase would add its inhibitory effect on GS to that of phosphorylation by the activated PhK (22).

The link between the high activity of GSK3β and diabetes in human skeletal muscle is well established (56), as is the therapeutic potential of GSK3β inhibitors (57,58). It is manifested in our patients by the correlation observed between content of activated kinase and FBS (supplemental Fig. 2 to Fig. 1). Regulation of GSk3β activity by proteolysis was first reported in the brain, where it was found associated with Tau hyperphosphorylation in Alzheimer's disease (29); the present study provides the first demonstration of its occurrence in skeletal muscle, where it leads to phosphorylation of glycogen synthase, as indicated by the correlation found between GSK3b cleavage and blood sugar.

Taken together, the present observations and those in ref. (22) identify a multi-lane pathway, where Ca^{2+} activation, proteolysis and phosphorylation, involving at a minimum calpain 1, GSK3β, GS, GP, PhK and GLUT4, lead from the primary Ca^{2+} dysregulation to hyperthermia and diabetes.

The Ca^{2+}-promoted cleavage of junctophilin 1 produces an adaptive transcription regulator

A decrease in levels of junctophilin associated with elevated $[Ca^{2+}]_{cyto}$ and activation of a calpain was first reported for cardiac muscle under the stress of heart failure, involving the tissue-specific junctophilin 2, JPh2, and calpain1 (59). Later, calpain2 was shown to also cleave JPh2 (26). The proteolysis of JPh2 was associated with structural remodeling, loss of dyadic junctions and deficit of EC coupling function, all expected from the breakage of a structural brace of the junction (60). Surprisingly, however, L-S Song's group went on to demonstrate that a large N-terminal calpain1-cleaved fragment of JPh2, named JPH2-NTP, entered nuclei, where it regulated transcription of multiple genes, with consequences that opposed the damaging effects of activated proteases (25). In contrast, Lahiri et al. (26) reported the presence of an ~25 kDa C-terminal product of cleavage by calpain2, which unlike JPH2-NTP was shown to be causative of cellular hypertrophy.

The present observations establish similarities and differences between the roles of JPh44 and those of the fragments described in cardiac muscle. The distribution of exogenous doubly tagged JPh1 and its fragments (Fig. 3A, C and Table 2) establishes that JPh44 is a C-terminal fragment. The calpain predictive algorithm, together with the observed distribution of the GFP-tagged Δ(1-240) JPh1, also establish with high likelihood the site of JPh1 cleavage, at either R240-S241 or S233-S234 (Fig. 4A). In addition to matching the apparent molecular weight of the endogenous JPh44, the C-terminal fragment resulting from cleavage at either point will contain two nuclear location sequences, allowing nuclear import of the fragment (Fig. 4A). Like JPH2-NTP, the fragment will have an alanine-rich region (ARR), with helix-turn-helix (HTH) structure, characteristic of DNA-binding proteins. These properties establish with near certainty the primary structure of JPh44 as the C-terminal fragment of JPh1 that starts at S241 or S234. We used this identification to directly probe the possible roles of JPh44. in adult mice muscle and C2C12 myoblasts. When expressed in muscle of adult mice, the GFP-tagged Δ(1-240) JPh1 appeared located similarly as JPh44 in human muscle, largely within the I band and inside nuclei, eschewing triadic junctions and colocalization with its marker, RyR1 (Fig. 8B-D and Table 1).

In C2C12 myoblasts, the construct likewise distributed inside nuclei, as well as in a fine-grained cytosolic form (Fig. 9A). Consistent with a gene regulatory role of GFP-tagged Δ(1-240) JPh1, the transcription profile of transfected myoblasts showed significant alterations in multiple pathways (9B, C). Notably, we found significantly reduced mRNA levels of GSK3β and four proteins that act as brakes on the PI3k-AKT pathway, namely Traf3 (TNF receptor-associated factor 3), Ces3a (carboxylesterase 3A), Repin1 (replication initiator 1) and Pck1 (phosphoenolpyruvate carboxykinase 1, PEPCK-C).

Among the many signaling pathways regulated by Akt, glucose uptake by muscle (and fat cells) is of particular interest here. In muscle, Akt isoform 2 is activated via phosphorylation by a chain of events at the plasma membrane started in response to insulin (61); this activation promotes translocation of GLUT4 to the plasma

membrane, enabling its transport role. Phosphorylation by Akt also inactivates GSK3β, which in turn releases glycogen synthase from inactivation, promoting storage of glucose. Hepatic and skeletal muscle silencing of the four genes named above improved the insulin resistance by inducing phosphorylation of Akt (62–65). Together, the effects on transcription of the exogenous JPh1 fragment are consistent with a beneficial, "stress-adaptive" role of the endogenous JPh44, similar to that ascribed to JPH2-NTP in stressed myocardium (25).

In spite of the similarity, there are many differences between the putatively regulatory fragments of the two junctophilin isoforms. Unlike JPH2-NTP, JPh44 loses an N-terminal portion and with it the main stretch of MORN motifs. Unlike JPH2-NTP, it retains both the transmembrane domain (TMD) and a second NLS (K588-L614, Fig. 4A). Therefore, the skeletal muscle fragment appears to have advantages over JPH2-NTP, both to leave the junctional location (by losing most MORN T-membrane anchors), and to reach inside nuclei, both by retaining its TMD, which allows it to follow a vesicular trafficking path, and by having an additional nuclear location sequence. In view of recent advances in understanding the molecular determinants of the tertiary structure of JPh isoforms 1 and 2 (40), cleavage of an N-terminal fragment that includes most MORN motifs would release the helical region from detailed, presumably tight association with the β sheet formed by the MORNs, freeing the helix for its putative interactions with DNA inside nuclei. In spite of these apparent advantages, the transcriptional changes ascribed to JPH2-NTP affect a greater number of genes (25), a difference that might be explained by the use of different preparations to evaluate the effects of the two protein fragments.

An additional, interesting difference between the MHS condition and the stress of heart failure, reported to unleash calpain cleavage of JPh2, is that the cardiac condition is accompanied by structural remodeling with loss of couplons and reduction in JPh2 content (60,66). By contrast, no structural remodeling in muscle of MHS patients has been reported, and the studies of Ca^{2+} release function revealed an increase in sensitivity to stimuli (membrane voltage or calcium) rather than the major deficits expected to arise from a loss of functional junctions. JPh1 is known to multimerize and JPh2 molecules are also present in skeletal muscle; as a result, the stoichiometry, the number of JPh1 molecules in T-SR junctions, is not known and may be variable, which leaves room for redundancy. It is possible that limited JPh1 cleavage in conditions of muscle stress causes minimal or no deterioration, structural or functional, while producing an adaptive, gene-regulatory messenger.

Conclusion

We report that the elevated $[Ca^{2+}]_{cyto}$ in skeletal muscle of individuals with MHS activates calpain1, which associates to T-SR junctions. The protease then cleaves a kinase that inhibits glycogen synthase, an effect that correlates with and probably contributes to an increase in blood glucose concentration. Cleavage of the kinase and that of GLUT4 promote the transition to hyperglycemia and diabetes found in many of these patients. It also cleaves junctophilin1, to produce a C-terminal fragment of ~44 kDa that abandons junctions and enters nuclei. There, the fragment modulates transcription of multiple genes, resulting in effects opposing the deleterious alteration of the glucose utilization pathway. Borrowing a term applied to a fragment of junctophilin2 found to enter nuclei in myocytes of failing hearts (25), the JPh44 fragment is therefore "stress-adaptive".

Methods

Patients

All patients were recruited, consented to all aspects of the study, and studied in the Malignant Hyperthermia Investigation Unit (MHIU) of the Canadian University Health Network, at Toronto General Hospital, in Toronto, Canada. Patients were diagnosed with the CHCT and studied over the last 5 years. Criteria for recruitment of subjects included one or more of the following: a previous adverse anesthetic reaction, family history of MH without a diagnostic MH mutation (www.emhg.org), a variant of unknown significance (VUS) in *RYR1* or *CACNA1S*, recurrent exercise- or heat-induced rhabdomyolysis and idiopathic elevation of serum creatine kinase.

Primary cultures

Biopsied segments of human *Gracilis* muscle were shipped to Rush University at 4°C overnight in an optimized solution of composition described in (21). Primary cultures, derived from the biopsies as described by Censier et al. (67), were maintained at 37°C in a humid atmosphere containing 5% CO_2. After 8–15 days, cells derived from the explants were transferred to a culture dish for proliferation in a growth medium. Myoblasts were expanded through up to four passages. For calcium concentration measurements in live cells, myoblasts were reseeded on collagen-coated dishes (MatTek, Ashland, MA, USA). For immunostaining experiments, myoblasts were seeded on 13 mm coverslips in 24 well plates. At 70% confluence, the cells were switched to a differentiation medium (DMEM-F12 with 2.5%horse serum). Studies were carried out 5–10 days thereafter, in myotubes showing a similar degree of maturation.

C2C12 cultures

The mouse myogenic C2C12 cell line was obtained from ATCC (http://www.atcc.org/) and cells were used until passage number 20. Myoblasts were cultured in Dulbecco's modified Eagle's medium (DMEM) supplemented with 15% fetal bovine serum and 1% penicillin-streptomycin in a humidified incubator kept at 37 °C and 5% CO_2. C2C12 myotubes were obtained by culturing 70% confluent myoblasts in differentiation medium (DMEM, 2% horse serum, 1% penicillin-streptomycin) for at least 4 days.

Transfections

Transient transfections of C2C12 myoblasts were performed upon reaching 70% confluence using the K2 Transfection System (Biontex Laboratories GmbH, Munich, Germany) as described by the manufacturer. C2C12 myotubes and biopsy-derived human primary myotubes were transfected with plasmids using lipofectamine 3000 (Thermofisher, Waltham, MA, USA) following the supplier's instructions.

Use of murine muscle

6–10 wk-old mice, *Mus musculus*, of the Black Swiss strain, sourced at Charles River Laboratories (Boston, MA, USA), were used to define the localization of JPh1 and JPh44 in living cells. Hind paws were transfected with plasmid vector for GFP-JPh1, dual tagged JPh1 plasmid (GFP-JPh1-FLAG), and GFP tagged plasmid with JPh44

translating region (GFP-Δ(1-240) JPh1) as described in (68). Animals were euthanized and muscles collected and processed for imaging as in (69).

Diagnosis of Malignant Hyperthermia Susceptibility

Susceptibility to MH was diagnosed at the MHIU following the North American CHCT protocol (Larach, 1989). Increases in baseline force in response to caffeine and halothane (F_C and F_H) were measured on freshly excised biopsies of *Gracilis* muscle with initial twitch responses that met viability criteria. Three muscle bundles were exposed successively to 0.5-, 1-, 2-, 4-, 8- and 32-mM caffeine; three separate bundles were exposed to 3% halothane. The threshold response for a positive diagnosis was either F_H ≥0.7 g or F_C (in 2-mM caffeine) ≥0.3 g. Patients were diagnosed as 'MH-negative' (MHN) if the increase in force was below threshold for both agonists, and 'MH-susceptible' (MHS) if at least one exposure exceeded the threshold. While prior work distinguishes the muscles that respond excessively to halothane but not to caffeine (named "HH") from those that respond to both (the "HS"), in the present work the distinction is not made, and both groups together are classified as MHS.

Cytosolic calcium concentration

Cytosolic Ca^{2+} concentration, $[Ca^{2+}]$cyto, was monitored in myotubes by shifted excitation and emission ratioing (70) of indo-1 fluorescence as described in (71). Imaging was by confocal microscopy (scanner TCS SP2; Leica Microsystems; Buffalo Grove, IL, USA), using a 63X 1.2 numerical-aperture water-immersion objective. $[Ca^{2+}]_{cyto}$ was derived from fluorescence signals (72). Indo-1 was procured from Invitrogen, Waltham, MA, USA.

Analysis of calpain activity

For in vitro JPh1 cleavage experiments, the whole biopsied muscles from human subjects were homogenized in RIPA lysis buffer (Santa Cruz Biotechnology, Dallas, TX, USA) with protease and phosphatase inhibitors, and the supernatant of centrifugation at 13,000 g for 15 min was used for further process. The cleavage of JPh1 was induced by incubating 100 micrograms of protein supernatants with 0.3–1.0 µg of purified human erythrocyte calpain1 of activity 1 unit/µg (MilliporeSigma, Burlington, MA, USA) at 30^0C for 15 minutes. Supernatants are treated with or without DMSO dissolved 10 µg calpain inhibitor (MDL28170, Cayman Chemical Co., Ann Arbor, MI, USA). SDS sample buffer was added to stop the reaction.

Protein fractionation and Western blotting

Human biopsied muscle segments received from the MHIU were quick-frozen for biochemical studies and storage. For measuring total content of proteins in muscle, the tissue was chopped into small pieces in RIPA lysis buffer (Santa Cruz Biotechnology, Dallas, TX, USA) containing protease and phosphatase inhibitors, and homogenized using a Polytron disrupter. The homogenate was centrifuged at 13000 g for 10 min and supernatant aliquots were stored in liquid nitrogen. Nuclear and cytosolic protein fractions from muscle biopsies were prepared using NE-PER™ Nuclear and Cytoplasmic Extraction Kit (Catalog. No 78835; ThermoFisher) according to the manufacturer instructions with the help of Dounce homogenizer.

Protein content was quantified by the BCA assay (ThermoFisher). Proteins were separated by SDS–polyacrylamide gel electrophoresis, using 10% mini gels and 26-well pre-cast gels (Criterion TGX, Bio-Rad, Hercules, CA, USA),

which enable separation in a broad range of molecular weights, and transferred to a nitrocellulose membrane (Bio-Rad). Membranes were blocked at 4.5% blotting grade (Bio-Rad) in PBS and incubated with the primary antibody overnight at 4°C. Thereafter they were washed in PBS containing 0.1% Tween 20 and incubated in horseradish peroxidase–conjugated anti-mouse or anti-rabbit secondary (Invitrogen, Carlsbad, CA, USA) for 1 hr at room temperature. The blot signals were developed with chemiluminescent substrate (MilliporeSigma) and detected using the Syngene PXi system (Syngene USA Inc, Frederick, MD, USA). Immunoblot analysis was conducted using the following antibodies (antigen, commercial ID number, concentration, supplier): JPh1 "antibody A", #PA5-52639, 1:1000, ThermoFisher; JPh1 "antibody B", #40-5100, 1:1000, ThermoFisher; GSK3β , #9315, 1:1000, Cell Signaling Technology (Danvers, MA, USA); calpain1, #MA1-12454, 1:1000, ThermoFisher; histone H3, #4499, 1:1000, Cell Signaling.

Quantitative analysis of Western blots was done with a custom application (written in the IDL platform, Harris Geospatiale, Paris, France; fully described and demonstrated with video in (22)) that combined information in the blot and the source gel. This method had less variance than the commercial (Syngene) software tools. The content of interest was measured in the blot by the signal mass within a rectangle that enclosed the protein band above a background. A normalization factor, quantifying the sample deposited in the lane, was computed on the gel as the average signal in a large area of the corresponding lane above background. A more advanced version was developed to automatically quantify closely-spaced dual bands (as in Fig. 4E); its use is illustrated in supplemental Fig. 1 to Fig. 4.

Two anti-JPh1 antibodies, A and B, both supplied by ThermoFisher, serendipitously showed different reactivity. When used in Western blots, antibody A (#PA5-52639) reacted almost exclusively with the full-size, ~72 kDa molecule (e.g., Fig.1 A), while antibody B (#40-5100) marked exclusively JPh44 (supplemental Fig. 1 to Fig. 1). This distinctive reactivity was reproduced in staining of adult muscle (e.g., compare panels Ab and Bb in Fig. 2), but not in myotubes, where antibody A stained both junctophilin forms (e.g., Fig. 2 Db) while antibody B retained its specific reactivity for JPh44 (e.g., Fig. 2 Eb).

Immunostaining of human and mice myofibers, and skeletal muscle cell cultures

Immunofluorescence imaging was done on thin myofiber bundles dissected from human muscle biopsies, FDB muscles from mice, primary human myotubes, C2C12-line myotubes and C2C12 myoblasts. Human or mouse muscles were mounted moderately stretched in relaxing solution, on Sylgard-coated dishes. Relaxing solution was replaced by fixative containing 4% PFA for 20 min. Myotubes or myoblasts on coverslips were washed in 1X PBS and fixed with 2% PFA for 20 min. Tissues or cell cultures on coverslips were transferred to a 24-well plate and washed three times for 10 min in PBS, then permeabilized with 0.1% Triton X-100 (Sigma) for 30 min at room temperature and blocked in 5% goat serum (Sigma) with slow agitation for 1 hr. The primary antibody was applied overnight at 4°C with agitation, followed by 3 PBS washes for 10 min. Fluorescent secondary antibody was applied for 2 hr at room temperature. Dehydrated tissues or cell culture coverslips were mounted with anti-fade medium (Prolong Diamond, ThermoFisher). Immunofluorescence imaging used the following antibodies (antigen,

commercial ID number, concentration, supplier): JPh1 “antibody A”, #PA5-52639, 1:100, ThermoFisher; JPh1 “antibody B”, #40-5100, 1:100, ThermoFisher; calpain1, #MA1-12454, 1:1000, ThermoFisher; Ryr1, #34C, 1:200, ThermoFisher.

High-Resolution imaging of fluorescence

Immunostained myofibers and cell cultures, as well as live tissues expressing fluorescently tagged proteins were imaged confocally using a Falcon SP8 laser scanning system (Leica Microsystems) with a 1.2-numerical aperture, water-immersion, 63x objective. Resolution was enhanced by high sensitivity hybrid GaAsP detectors (HyD, Leica), which allowed low intensity illumination for image averaging with minimum bleaching, optimal confocal pinhole size (below 1 Airy disk), collection of light in extended ranges (e.g., 470-580 nm), and acquisition of *z*-stacks (vertical sets of x-y images) at oversampled *x–y–z* intervals. The stacks usually included 40 x-y images at 120 nm z separation and 60 nm x-y pixel size or, for highest resolution imaging, 20 x-y images at 120 nm z and 36 nm x-y pixel size. Dual images were interleaved by line. Most cells were triply stained and correspondingly monitored at (excitation/emission) (405/ 430-470 nm), (488/500–550 nm) and (555/570–620 nm). The stacks were acquired starting nearest the objective, at or closely outside the lower surface of the myofiber.

Availability of stacks allowed for offline deblurring by a constrained iterative deconvolution algorithm that used all images in the stack (73,74) and the point spread function (PSF) of the system, which was determined using 170-nm beads. PSF FWHM was 350 nm in *x–y* and 480 nm in *z*. After deblurring, the separation effectively resolved in the x-y plane was approximately 0.1 µm (Supplement 11 in (22)). The deblurred set was represented or “rendered” in three dimensions using the “Simulated Fluorescence Process” (75) applied to the full deblurred stack. Determination of the point spread function (PSF) of the imaging system, deblurring, and rendering were done in the HuPro (SVI, Amsterdam, The Netherlands) programming environment.

Location and colocalization analyses

Location analysis defined densities of protein content within nuclei or in extra-nuclear areas (named “cytosol”), by the ratio of integrated fluorescence signal over area in the respective regions. For comparisons among replications the ratio (nuclear/cytosolic) was used, as it was insensitive to inter-preparation variance in expression or staining intensity.

Colocalization (of JPh1, its fragment JPh44, its expressed constructs GFP-JPh1-FLAG, (N)Myc-JPh1 and GFP-Δ(1-240)JPh1, calpain1, its expressed construct (N)FLAG-calpain1 and RyR1) was evaluated by 4 techniques: (1) the Pearson correlation coefficient, calculated as:

$$R = \frac{\sum_i \left(A_i - \overline{A}_i\right)\left(B_i - \overline{B}_i\right)}{\sqrt{\left(A_i - \overline{A}_i\right)^2 \left(B_i - \overline{B}_i\right)^2}} \tag{1}$$

where A_i and B_i are intensities of two signals in the same pixel i, $\overline{A}_i$ and $\overline{B}_i$ the averages over all pixels, and the summation is extended to all pixels, or a ROI when the entire image is not usable. Subtler, but statistically

significant differences in colocalization were detected using the Intensity Correlation Analysis (ICA) introduced by Li et al. (32). This analysis produces a quantitative measure, the Intensity Correlation Quotient, ICQ, a correlation measure with a definition that reduces the influence of heterogeneous staining of protein expression.

$$ICQ = \frac{\sum_i Sign\left[\left(A_i - \bar{A}_i\right)\left(B_i - \bar{B}_i\right)\right]}{N(pixels)} - 0.5 \qquad (2)$$

The numerator contributes a 1 for every pixel where both signals are above or below average and a -1 for the situation where the differences are opposite. The ratio is normalized to 1 and the subtraction of 0.5 moves the range to [-0.5, 0.5], with the extremes corresponding to perfect exclusion and perfect colocalization. The ICA approach includes a graph, (with examples in panels Fig. 2Cb, d), that plots for every pixel the product $\left(A_i - \bar{A}_i\right)\left(B_i - \bar{B}_i\right)$, or "pixel covariance" of A and B, vs. the intensity of either A or B. The result is strikingly different for cases of colocalization, where the points draw a noisy parabola (e.g., 2Cb) or lack of it (e.g., 2Cd), where points to the left of the abscissa 0 correspond to mutual exclusion of the two signals.

The conventional correlation analyses have no provision for identifying the anisotropic de-localization of particles, which, if systematic, may reflect an actual association, with systematic displacement. This sensitivity to vectorial displacement is achieved here using an approach of Van Steensel et al. (33), which again produces a plot and, in this case, two numerical outputs of interest. The approach (illustrated in Fig. 2 Ca, c) plots the correlation coefficient *R* between image A and image B shifted in one direction (say, *x*, defined as the longitudinal direction in myofibers) by variable amounts *dx*. The "Van Steensel plot" thus plots *R* (*dx*) vs. *dx*. represented by individual symbols in Fig. 2Ca. When the two signals are colocalized, the plot is narrow, and centered at dx = 0. If not, the plot displaces its peak (when the delocalization occurs in a preferred direction) and its width increases. Two numerical quantifiers can be derived on a Gaussian fitted to the points: the abscissa of the maximum (here the "VS shift") and the FWHM. These quantifiers reveal vectorial aspects of the relationship between the two markers. The VS shift gives a rough measure of distance when the separation of the molecules has some vectorial regularity and sidedness. The FWHM is a measure of dispersion of one marker or both. Combined with the high spatial resolution achieved in our images, it allows to detect effects of interventions that fail to cause significant changes by conventional colocalization measurements.

Colocalization measures and plots were implemented with custom programs written in the IDL platform or with the ImageJ "plugin" JACoP (76).

Replications and Statistics

With few exceptions, due to limitations in the availability of human samples or their derived cultures, imaging and quantitative analyses were replicated in multiple cells from multiple individuals. In figures and tables, the numbers of individuals (patients, mice) is represented by N and the total numbers of cells by n. When multiple cells derive from multiple individuals, statistical measures are derived by hierarchical (nested) analysis implemented in the R environment (77). Significance of differences of averages or paired differences is

established using the two-tailed Student's t test, or, when the distributions of compared measures are do not satisfy tests of normality and equal variance, the Mann-Whitney Rank Sum test. Correlation between variables is quantified by the first-order correlation coefficient R; this number is always accompanied by an estimate p of the probability of no correlation, a function of R and the sample size, is calculated as described in (22). In tables, sample medians are always provided after sample averages, to afford a first idea of the distribution.

Supplement

Supplemental materials include: a PDF document with untrimmed versions of all Western blots and their originating, Ponceau-stained gels, which were used for normalization of the WB bands, two supplemental figures to Fig. 1 and two to Fig. 4.

Raw data

All quantitative raw data are contained in "JNB" (Sigmaplot) and "XLSX" (Excel) annotated worksheets, available in depository. To allow referencing and use of the data, a "data trace" paragraph is added to every figure and table legend. Original images are 3-dimensional arrays, of size ~100 MB, available upon justified request.

Digital gene expression sequencing

RNA was isolated from GFP-empty vector-transfected and GFP-Δ(1-240) JPh1-transfected C2C12 myoblasts using the RNeasy plus mini kit (Qiagen, Hilden, Germany), based on manufacturer instructions . Samples were processed by LC Sciences (Houston,TX, USA). Processing included the generation of a library and sequencing of transcripts and their identification in the mouse genome (UCSC mm10). A cDNA library constructed from the pooled RNA from C2C12 cell samples of mouse species was sequenced run with Illumina Novaseq TM 6000 sequence platform. Raw paired-end RNA-seq data were firstly subjected to Cutadapt v1.9 to remove reads with adaptor contamination, low quality bases and undetermined bases. Filtered reads were aligned using HISAT2 to generate alignments tailored for transcript assembler. The mapped reads of each sample were assembled using StringTie with default parameters. Then, all transcriptomes from all samples were merged to reconstruct a comprehensive transcriptome using Gffcompare. After the final transcriptome was generated, StringTie and Ballgown were used to estimate the expression levels of all transcripts and perform expression abundance for mRNAs, by calculating FPKM (fragment per kilobase of transcript per million mapped reads). Differential expression analysis was performed by DESeq2 software between two groups. The genes with the parameter of false discovery rate (FDR) below 0.05 and absolute fold change ≥ 2 were considered differentially expressed. Differentially expressed genes were then subjected to enrichment analysis of GO functions and KEGG pathways.

Study approval

Following approval by the institutional Research Ethics Board of Toronto General Hospital (TGH), informed consents were obtained from all patients who underwent the CHCT. The consent, also approved by the Institutional Review Board of Rush University, included use of biopsies for functional studies, imaging and cell culture. Ethical aspects of the animal studies were approved by the IACUC of Rush University.

Supplemental Figures

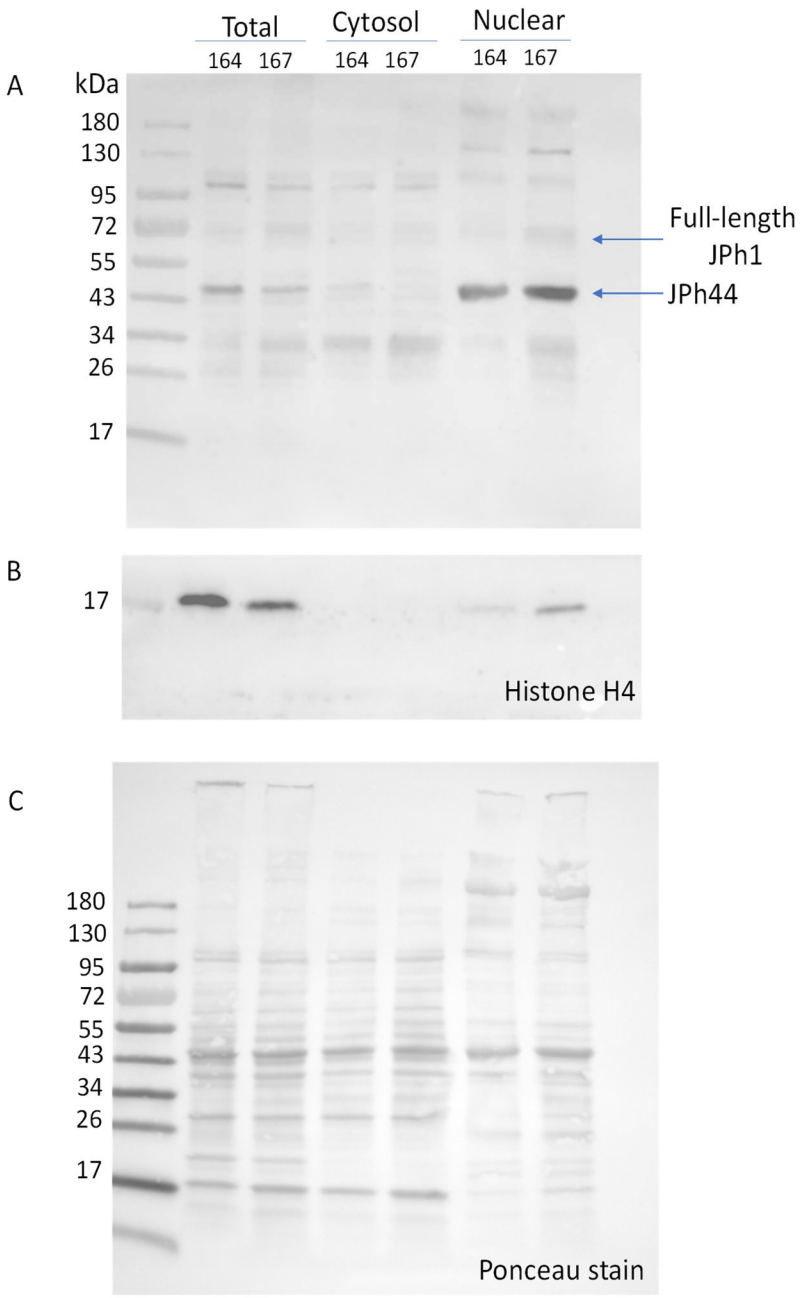

Supp. Fig. 1 to Fig. 1. JPh1 "antibody B" (details in Methods) detects predominantly JPh44. A, Western blot of protein extract from full-tissue, cytosol or nuclear fraction of muscle of two patients, stained with anti-JPh1 antibody B. B, same fractions stained for histone H4 (a nuclear marker). C, Ponceau stain of electrophoresed gel, showing fairly uniform loading, allows direct visual comparison of bands in A and B. The cytosol fraction, which does not to contain nuclear material (according to histone staining), has essentially no JPh1 signal. This is in contrast with the intense signal from antibody A, displayed in Fig. 1A. The difference demonstrates the high specificity of antibody B for the JPh44 fragment. Patient identifiers: #164 (diagnosed as MHN) and #167 (MHS).

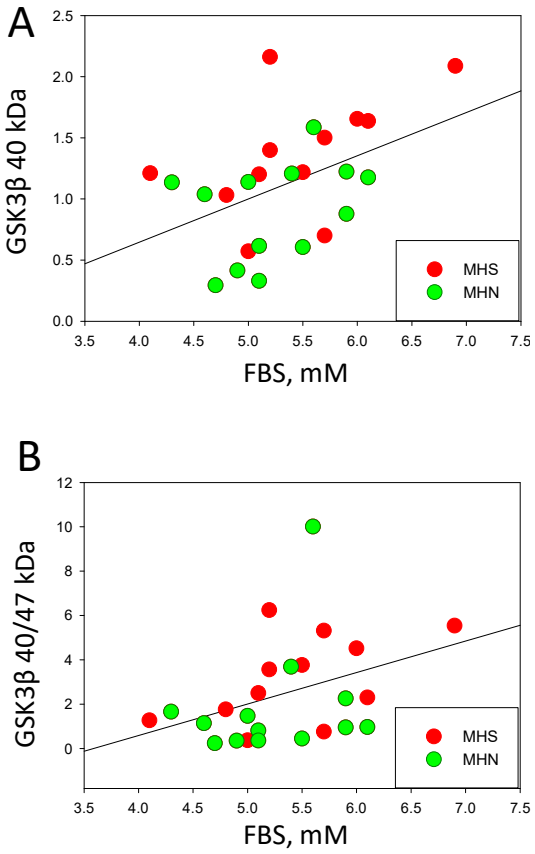

Supp. Fig. 2 to Fig. 1. Plots of Fasting Blood Glucose (FBS) measured in the 25 patients with analysis of GSK3β analysis reported in Fig. 1, vs. the normalized content of truncated (activated) GSK3β (panel A), or the truncated/full-size ratio of contents (panel B). The variables are positively correlated; R = 0.45 for panel A and 0.38 for panel B. The probabilities p of no correlation are 0.02 and 0.06, respectively.

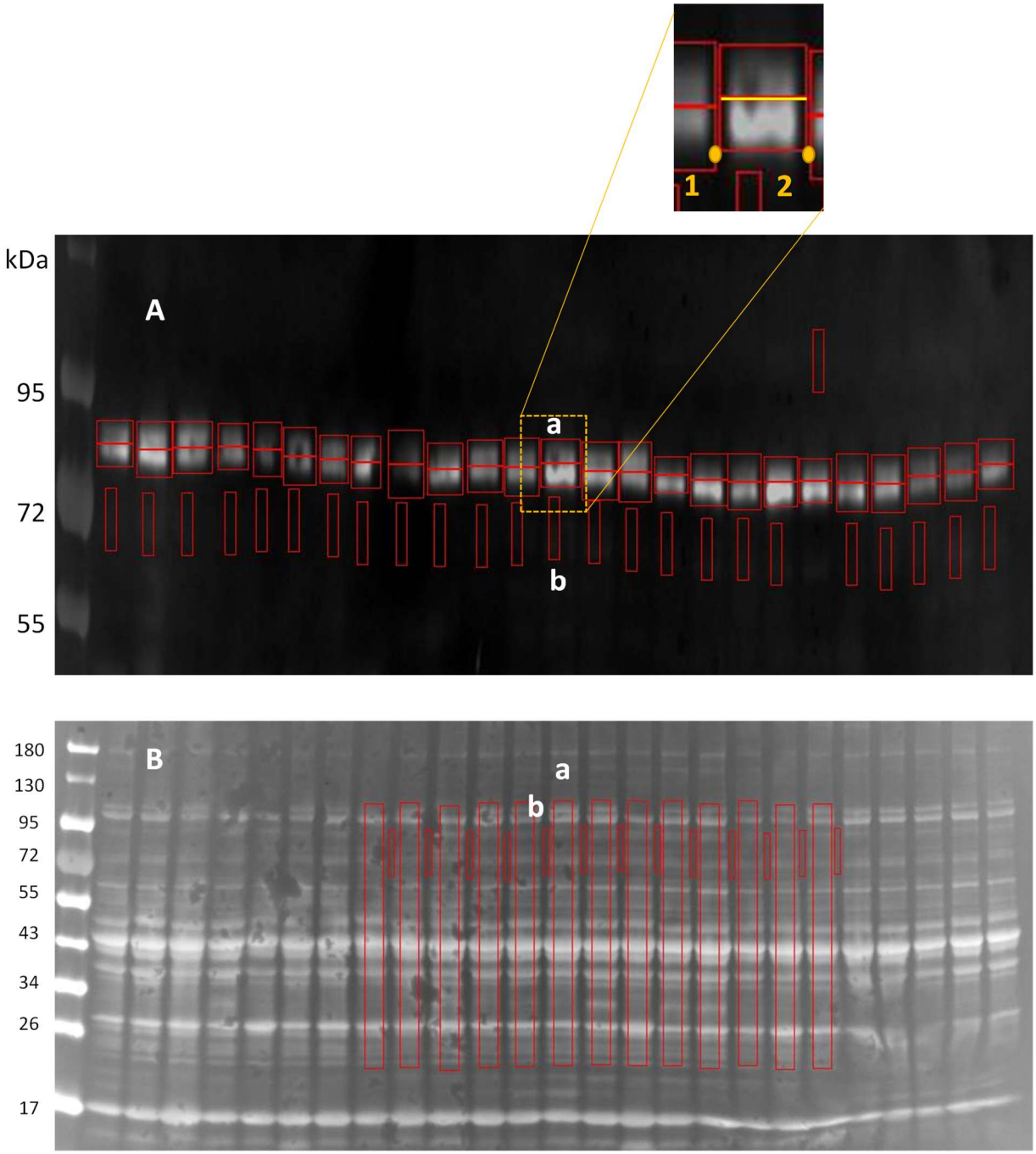

Supp. Fig. 1 to Fig. 4. A streamlined method to quantify double bands in Western blots. The method introduced by Tammineni et al. in (22) was modified for objective analysis of closely placed double bands. A, Western blot, stained for calpain1 (reproduced from Fig. 4E, at 4x magnification in the vertical direction, converted to "positive", i.e., with pixel values corresponding to reporter intensity signal), shows closely placed bands at approx. 80 and 76 kDa. B, the originating gel, at the original magnification. On WB (panel A), working on one column at a time, the user selects a background region "b" and starts the definition of two active region of interest (ROIs) "a" by marking points 1 and 2 (inset), which define the width of the ROIs. The program then locates automatically a border between the two close bands (yellow segment), at the minimum of the bands signal, averaged in the horizontal direction. Two symmetrical ROIs (red rectangles) are thus defined, where the signals of the two bands are integrated. For normalization to total quantity of protein, the signals are then normalized by the total signal in the corresponding column of the Ponceau-stained gel, calculated as the difference between the signal integrated over active area "a" (in B), after subtraction of background "b". All ROIs "a" in B have the same area. For columns where the minimum used to define the border in A is ill-defined, the user may set the border between the two bands by eye. Program code, written in the IDL environment (Geospatiale, Paris, France), is available upon request.

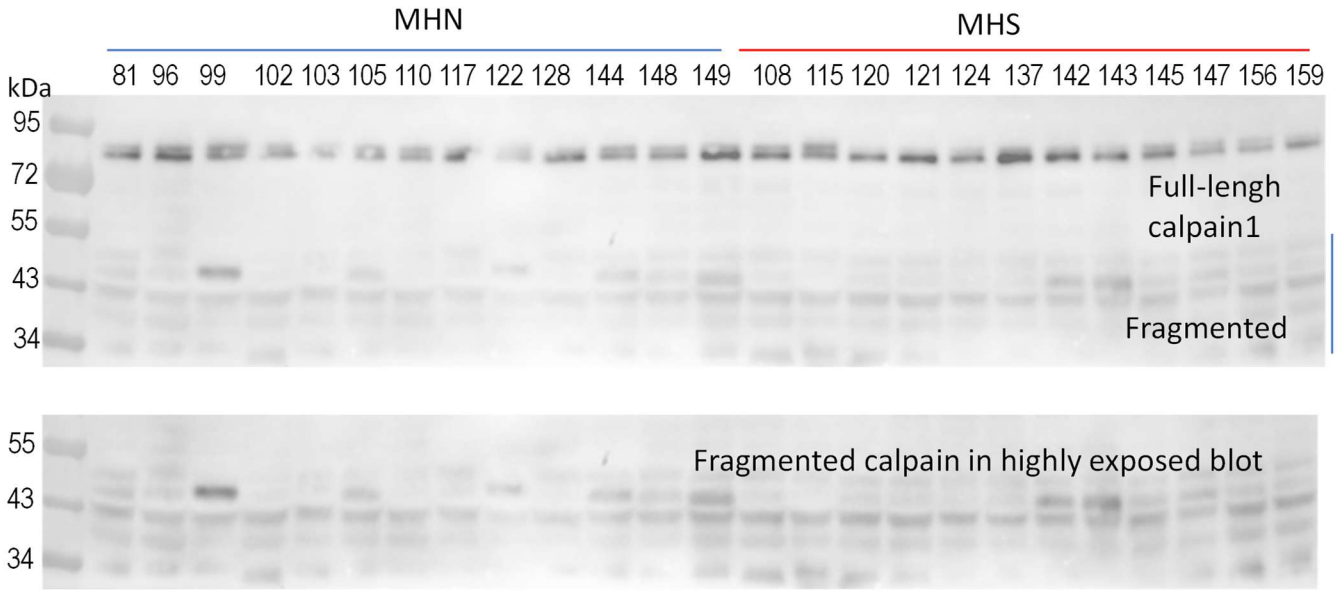

Supp. Fig. 2 to Fig.4. Western blot of calpain1 in whole-tissue protein of human subjects. Same as in Fig. 4 E, extending range to show multiple low-weight fragments. The region of fragments is shown in the bottom panel, developed at higher exposure.

References

1. Stern MD, Pizarro G, Ríos E. Local control model of excitation-contraction coupling in skeletal muscle. J Gen Physiol. 1997 Oct;110(4):415–40.

2. Franzini-Armstrong C, Protasi F, Ramesh V. Shape, size, and distribution of Ca(2+) release units and couplons in skeletal and cardiac muscles. Biophys J. 1999 Sep;77(3):1528–39.

3. Perni S, Lavorato M, Beam KG. De novo reconstitution reveals the proteins required for skeletal muscle voltage-induced Ca2+ release. Proc Natl Acad Sci U S A. 2017 26;114(52):13822–7.

4. Wu F, Quiñonez M, DiFranco M, Cannon S. Stac3 enhances expression of human CaV1.1 in Xenopus oocytes and reveals gating pore currents in HypoPP mutant channels. J Gen Physiol. 2018;

5. Takeshima H, Komazaki S, Nishi M, Iino M, Kangawa K. Junctophilins: a novel family of junctional membrane complex proteins. Mol Cell. 2000 Jul;6(1):11–22.

6. Komazaki S, Ito K, Takeshima H, Nakamura H. Deficiency of triad formation in developing skeletal muscle cells lacking junctophilin type 1. FEBS Lett. 2002 Jul 31;524(1–3):225–9.

7. Rossi D, Scarcella AM, Liguori E, Lorenzini S, Pierantozzi E, Kutchukian C, et al. Molecular determinants of homo- and heteromeric interactions of Junctophilin-1 at triads in adult skeletal muscle fibers. Proc Natl Acad Sci U S A. 2019 30;116(31):15716–24.

8. Litman RS, Griggs SM, Dowling JJ, Riazi S. Malignant Hyperthermia Susceptibility and Related Diseases. Anesthesiology. 2018;128(1):159–67.

9. Ríos E, Figueroa L, Manno C, Kraeva N, Riazi S. The couplonopathies: A comparative approach to a class of diseases of skeletal and cardiac muscle. J Gen Physiol. 2015 Jun;145(6):459–74.

10. Dirksen RT, Avila G. Distinct effects on Ca2+ handling caused by malignant hyperthermia and central core disease mutations in RyR1. Biophys J. 2004 Nov;87(5):3193–204.

11. Lopez JR, Alamo LA, Jones DE, Papp L, Allen PD, Gergely J, et al. [Ca2+]i in muscles of malignant hyperthermia susceptible pigs determined in vivo with Ca2+ selective microelectrodes. Muscle Nerve. 1986 Jan;9(1):85–6.

12. Lopez JR, Gerardi A, Lopez MJ, Allen PD. Effects of dantrolene on myoplasmic free [Ca2+] measured in vivo in patients susceptible to malignant hyperthermia. Anesthesiology. 1992 May;76(5):711–9.

13. Eltit JM, Hidalgo J, Liberona JL, Jaimovich E. Slow calcium signals after tetanic electrical stimulation in skeletal myotubes. Biophys J. 2004 May;86(5):3042–51.

14. Eltit JM, Ding X, Pessah IN, Allen PD, Lopez JR. Nonspecific sarcolemmal cation channels are critical for the pathogenesis of malignant hyperthermia. FASEB J Off Publ Fed Am Soc Exp Biol. 2013 Mar;27(3):991–1000.

15. Manno C, Figueroa L, Royer L, Pouvreau S, Lee C-S, Volpe P, et al. Altered Ca2+ concentration, permeability and buffering in the myofiber Ca2+ store of a mouse model of malignant hyperthermia. J Physiol. 2013 Jul 29;

16. Ríos E. The cell boundary theorem: a simple law of the control of cytosolic calcium concentration. J Physiol Sci JPS. 2010 Jan;60(1):81–4.

17. Edwards JN, Friedrich O, Cully TR, von Wegner F, Murphy RM, Launikonis BS. Upregulation of store-operated Ca2+ entry in dystrophic mdx mouse muscle. Am J Physiol Cell Physiol. 2010 Jul;299(1):C42-50.

18. Boittin F-X, Petermann O, Hirn C, Mittaud P, Dorchies OM, Roulet E, et al. Ca2+-independent phospholipase A2 enhances store-operated Ca2+ entry in dystrophic skeletal muscle fibers. J Cell Sci. 2006 Sep 15;119(Pt 18):3733–42.

19. Bellinger AM, Reiken S, Carlson C, Mongillo M, Liu X, Rothman L, et al. Hypernitrosylated ryanodine receptor calcium release channels are leaky in dystrophic muscle. Nat Med. 2009 Mar;15(3):325–30.

20. Britt BA. Malignant Hyperthermia: A Review. In: Thermoregulation: Pathology, Pharmacology and Therapy. New York: Pergamon Press; 1991. p. 179–292.

21. Figueroa L, Kraeva N, Manno C, Toro S, Ríos E, Riazi S. Abnormal calcium signalling and the caffeine-halothane contracture test. Br J Anaesth. 2019 Jan;122(1):32–41.

22. Tammineni E, Kraeva N, Figueroa N, Manno C, Ibarra C, Klip A, et al. Intracellular calcium leak lowers glucose storage in human muscle, promoting hyperglycemia and diabetes. eLife. 2020 May 4;2020:9:53999.

23. Altamirano F, Riazi S, Ibarra Moreno CA, Kraeva N, Uryash A, Allen PD, et al. Is malignant hyperthermia associated with hyperglycaemia? Br J Anaesth. 2019 Jan;122(1):e3–5.

24. Takeshima H, Hoshijima M, Song L-S. Ca^{2+} microdomains organized by junctophilins. Cell Calcium. 2015 Oct;58(4):349–56.

25. Guo A, Wang Y, Chen B, Wang Y, Yuan J, Zhang L, et al. E-C coupling structural protein junctophilin-2 encodes a stress-adaptive transcription regulator. Science. 2018 21;362(6421).

26. Lahiri SK, Quick AP, Samson-Couterie B, Hulsurkar M, Elzenaar I, van Oort RJ, et al. Nuclear localization of a novel calpain-2 mediated junctophilin-2 C-terminal cleavage peptide promotes cardiomyocyte remodeling. Basic Res Cardiol. 2020 26;115(4):49.

27. Ito K, Komazaki S, Sasamoto K, Yoshida M, Nishi M, Kitamura K, et al. Deficiency of triad junction and contraction in mutant skeletal muscle lacking junctophilin type 1. J Cell Biol. 2001 Sep 3;154(5):1059–67.

28. Michelucci A, Paolini C, Boncompagni S, Canato M, Reggiani C, Protasi F. Strenuous exercise triggers a life-threatening response in mice susceptible to malignant hyperthermia. FASEB J Off Publ Fed Am Soc Exp Biol. 2017 Aug;31(8):3649–62.

29. Jin N, Yin X, Yu D, Cao M, Gong C-X, Iqbal K, et al. Truncation and activation of GSK-3β by calpain I: a molecular mechanism links to tau hyperphosphorylation in Alzheimer's disease. Sci Rep. 2015 Feb 2;5(1):8187.

30. Goñi-Oliver P, Lucas JJ, Avila J, Hernández F. N-terminal Cleavage of GSK-3 by Calpain: A NEW FORM OF GSK-3 REGULATION *. J Biol Chem. 2007 Aug 3;282(31):22406–13.

31. Ma S, Liu S, Huang Q, Xie B, Lai B, Wang C, et al. Site-specific Phosphorylation Protects Glycogen Synthase Kinase-3β from Calpain-mediated Truncation of Its N and C Termini *. J Biol Chem. 2012 Jun 29;287(27):22521–32.

32. Li Q, Lau A, Morris TJ, Guo L, Fordyce CB, Stanley EF. A syntaxin 1, Galpha(o), and N-type calcium channel complex at a presynaptic nerve terminal: analysis by quantitative immunocolocalization. J Neurosci Off J Soc Neurosci. 2004 Apr 21;24(16):4070–81.

33. van Steensel B, van Binnendijk EP, Hornsby CD, van der Voort HT, Krozowski ZS, de Kloet ER, et al. Partial colocalization of glucocorticoid and mineralocorticoid receptors in discrete compartments in nuclei of rat hippocampus neurons. J Cell Sci. 1996 Apr;109 (Pt 4):787–92.

34. Figueroa L, Kraeva N, Manno C, Riazi S, Rios E. Differential Sensitivity to Halothane Among Subgroups of Malignant Hyperthermia Susceptible Patients: Insights into Dual Pathophysiological Mechanisms. Biophyscial J. 2021;120(3):150a–1a.

35. Yoshimura N, Kikuchi T, Sasaki T, Kitahara A, Hatanaka M, Murachi T. Two distinct Ca2+ proteases (calpain I and calpain II) purified concurrently by the same method from rat kidney. J Biol Chem. 1983 Jul 25;258(14):8883–9.

36. Goll DE, Thompson VF, Li H, Wei W, Cong J. The calpain system. Physiol Rev. 2003 Jul;83(3):731–801.

37. SUZUKI K, TSUJI S, ISHIURA S, KIMURA Y, KUBOTA S, IMAHORI K. Autolysis of Calcium-Activated Neutral Protease of Chicken Skeletal Muscle1. J Biochem (Tokyo). 1981 Oct 1;90(6):1787–93.

38. Moldoveanu T, Hosfield CM, Lim D, Elce JS, Jia Z, Davies PL. A Ca2+ Switch Aligns the Active Site of Calpain. Cell. 2002 Mar 8;108(5):649–60.

39. Liu Z, Cao J, Gao X, Ma Q, Ren J, Xue Y. GPS-CCD: a novel computational program for the prediction of calpain cleavage sites. PloS One. 2011 Apr 20;6(4):e19001.

40. Yang ZF, Panwar P, McFarlane CR, Tuinte WE, Campiglio M, Van Petegem F. Structures of the junctophilin/voltage-gated calcium channel interface reveal hot spot for cardiomyopathy mutations. Proc Natl Acad Sci. 2022 Mar 8;119(10):e2120416119.

41. Murphy RM, Verburg E, Lamb GD. Ca2+ activation of diffusible and bound pools of mu-calpain in rat skeletal muscle. J Physiol. 2006 Oct 15;576(Pt 2):595–612.

42. Murphy RM. Calpains, skeletal muscle function and exercise. In 2009. Available from: http://aups.org.au/Proceedings/40/95-102/#13

43. Goll DE, Thompson VF, Taylor RG, Christiansen JA. Role of the calpain system in muscle growth. Biochimie. 1992 Mar;74(3):225–37.

44. Wan F, Letavernier E, Abid S, Houssaini A, Czibik G, Marcos E, et al. Extracellular Calpain/Calpastatin Balance Is Involved in the Progression of Pulmonary Hypertension. Am J Respir Cell Mol Biol. 2016 Sep;55(3):337–51.

45. Patel S, Doble BW, MacAulay K, Sinclair EM, Drucker DJ, Woodgett JR. Tissue-Specific Role of Glycogen Synthase Kinase 3β in Glucose Homeostasis and Insulin Action. Mol Cell Biol. 2008 Oct 15;28(20):6314–28.

46. DeFronzo RA, Tripathy D. Skeletal muscle insulin resistance is the primary defect in type 2 diabetes. Diabetes Care. 2009 Nov;32 Suppl 2:S157-163.

47. Place N, Ivarsson N, Venckunas T, Neyroud D, Brazaitis M, Cheng AJ, et al. Ryanodine receptor fragmentation and sarcoplasmic reticulum Ca2+ leak after one session of high-intensity interval exercise. Proc Natl Acad Sci. 2015 Dec 15;112(50):15492–7.

48. Ashida Y, Himori K, Tamai K, Kimura I, Yamada T. Preconditioning contractions prevent prolonged force depression and Ca2+-dependent proteolysis of STAC3 after damaging eccentric contractions. J Appl Physiol Bethesda Md 1985. 2021 Nov 1;131(5):1399–407.

49. Otani K, Han D-H, Ford EL, Garcia-Roves PM, Ye H, Horikawa Y, et al. Calpain system regulates muscle mass and glucose transporter GLUT4 turnover. J Biol Chem. 2004 May 14;279(20):20915–20.

50. Dowling JJ, Lawlor MW, Dirksen RT. Triadopathies: an emerging class of skeletal muscle diseases. Neurother J Am Soc Exp Neurother. 2014 Oct;11(4):773–85.

51. Lawal TA, Todd JJ, Witherspoon JW, Bönnemann CG, Dowling JJ, Hamilton SL, et al. Ryanodine receptor 1-related disorders: an historical perspective and proposal for a unified nomenclature. Skelet Muscle. 2020 Nov 16;10(1):32.

52. Leon LR, Bouchama A. Heat stroke. Compr Physiol. 2015 Apr;5(2):611–47.

53. Hopkins PM, Ellis FR, Halsall PJ. Evidence for related myopathies in exertional heat stroke and malignant hyperthermia. Lancet Lond Engl. 1991 Dec 14;338(8781):1491–2.

54. Turner RM, Pirmohamed M. Statin-Related Myotoxicity: A Comprehensive Review of Pharmacokinetic, Pharmacogenomic and Muscle Components. J Clin Med. 2019 Dec 20;9(1):22.

55. Brushia RJ, Walsh DA. Phosphorylase kinase: the complexity of its regulation is reflected in the complexity of its structure. Front Biosci J Virtual Libr. 1999 Sep 15;4:D618-641.

56. Henriksen EJ, Dokken BB. Role of glycogen synthase kinase-3 in insulin resistance and type 2 diabetes. Curr Drug Targets. 2006 Nov;7(11):1435–41.

57. Dokken BB, Henriksen EJ. Chronic selective glycogen synthase kinase-3 inhibition enhances glucose disposal and muscle insulin action in prediabetic obese Zucker rats. Am J Physiol Endocrinol Metab. 2006 Aug;291(2):E207-213.

58. Maqbool M, Hoda N. GSK3 Inhibitors in the Therapeutic Development of Diabetes, Cancer and Neurodegeneration: Past, Present and Future. Curr Pharm Des. 2017 Nov 16;23(29):4332–50.

59. Guo A, Zhang C, Wei S, Chen B, Song L-S. Emerging mechanisms of T-tubule remodelling in heart failure. Cardiovasc Res. 2013 May 1;98(2):204–15.

60. Wu CC, Chen B, Jiang Y, Jia Z, Martin DW, Liu S, et al. Calpain-Dependent Cleavage of Junctophilin-2 and T-Tubule Remodeling in a Mouse Model of Reversible Heart Failure. J Am Heart Assoc. 3(3):e000527.

61. Boucher J, Kleinridders A, Kahn CR. Insulin Receptor Signaling in Normal and Insulin-Resistant States. Cold Spring Harb Perspect Biol. 2014 Jan;6(1):a009191.

62. Chen Z, Canet MJ, Sheng L, Jiang L, Xiong Y, Yin L, et al. Hepatocyte TRAF3 promotes insulin resistance and type 2 diabetes in mice with obesity. Mol Metab. 2015 Oct 17;4(12):951–60.

63. Lian J, Quiroga AD, Li L, Lehner R. Ces3/TGH deficiency improves dyslipidemia and reduces atherosclerosis in Ldlr(-/-) mice. Circ Res. 2012 Sep 28;111(8):982–90.

64. Kern M, Kosacka J, Hesselbarth N, Brückner J, Heiker JT, Flehmig G, et al. Liver-restricted Repin1 deficiency improves whole-body insulin sensitivity, alters lipid metabolism, and causes secondary changes in adipose tissue in mice. Diabetes. 2014 Oct;63(10):3295–309.

65. Gómez-Valadés AG, Méndez-Lucas A, Vidal-Alabró A, Blasco FX, Chillon M, Bartrons R, et al. Pck1 gene silencing in the liver improves glycemia control, insulin sensitivity, and dyslipidemia in db/db mice. Diabetes. 2008 Aug;57(8):2199–210.

66. Zhang H-B, Li R-C, Xu M, Xu S-M, Lai Y-S, Wu H-D, et al. Ultrastructural uncoupling between T-tubules and sarcoplasmic reticulum in human heart failure. Cardiovasc Res. 2013 May 1;98(2):269–76.

67. Censier K, Urwyler A, Zorzato F, Treves S. Intracellular calcium homeostasis in human primary muscle cells from malignant hyperthermia-susceptible and normal individuals. Effect Of overexpression of recombinant wild-type and Arg163Cys mutated ryanodine receptors. J Clin Invest. 1998 Mar 15;101(6):1233–42.

68. Pouvreau S, Royer L, Yi J, Brum G, Meissner G, Ríos E, et al. Ca(2+) sparks operated by membrane depolarization require isoform 3 ryanodine receptor channels in skeletal muscle. Proc Natl Acad Sci U S A. 2007 Mar 20;104(12):5235–40.

69. Manno C, Figueroa LC, Gillespie D, Fitts R, Kang C, Franzini-Armstrong C, et al. Calsequestrin depolymerizes when calcium is depleted in the sarcoplasmic reticulum of working muscle. Proc Natl Acad Sci U S A. 2017 Jan 24;114(4):E638–47.

70. Launikonis BS, Zhou J, Royer L, Shannon TR, Brum G, Ríos E. Confocal imaging of [Ca2+] in cellular organelles by SEER, shifted excitation and emission ratioing of fluorescence. J Physiol. 2005 Sep 1;567(Pt 2):523–43.

71. Zhou J, Yi J, Royer L, Launikonis BS, González A, García J, et al. A probable role of dihydropyridine receptors in repression of Ca2+ sparks demonstrated in cultured mammalian muscle. Am J Physiol Cell Physiol. 2006 Feb;290(2):C539-553.

72. Figueroa L, Shkryl VM, Zhou J, Manno C, Momotake A, Brum G, et al. Synthetic localized calcium transients directly probe signalling mechanisms in skeletal muscle. J Physiol. 2012 Mar 15;590(Pt 6):1389–411.

73. Van Der Voort HTM, Strasters KC. Restoration of confocal images for quantitative image analysis. J Microsc. 1995 May 1;178(2):165–81.

74. Agard DA, Hiraoka Y, Shaw P, Sedat JW. Fluorescence microscopy in three dimensions. Methods Cell Biol. 1989;30:353–77.

75. Messerli JM, van der Voort HT, Rungger-Brändle E, Perriard JC. Three-dimensional visualization of multi-channel volume data: the amSFP algorithm. Cytometry. 1993 Oct;14(7):725–35.

76. Bolte S, Cordelières FP. A guided tour into subcellular colocalization analysis in light microscopy. J Microsc. 2006 Dec;224(Pt 3):213–32.

77. Sikkel MB, Francis DP, Howard J, Gordon F, Rowlands C, Peters NS, et al. Hierarchical statistical techniques are necessary to draw reliable conclusions from analysis of isolated cardiomyocyte studies. Cardiovasc Res. 2017 Aug;113(14):1743–52.

Tables

				1	2	3	4
		N subjects	n, fibers or myotubes	R	VS shift, nm	FWHM, µm	ICQ
JPh44 in myofibers	average	3	10	0.31	66	0.56	0.22
	median			0.26	54	0.50	0.23
	S.E.M.			0.04	15	0.19	0.02
JPh1 in myofibers	average	3	8	0.88	16	0.42	0.4
	median			0.9	12	0.40	0.42
	S.E.M.			0.03	3	0.07	0.02
p				<0.001	<0.001	0.06	<0.001
JPh44 in myotubes	average	2	9	0.37	168	1.74	0.22
	median			0.36	164	1.69	0.22
	S.E.M.			0.05	36	0.17	0.03
JPh1 in myotubes	average	3	29	0.73	38	0.55	0.32
	median			0.77	38	0.50	0.32
	S.E.M.			0.02	4	0.03	0.01
p				<0.001	<0.001	<0.001	0.003

Table 1. Colocalization of JPh1 and its fragment with RyR1 in patients' muscle or patient-derived myotubes. Col. 1: Pearson's pixel-by-pixel correlation coefficient. 2: Van Steensel's shift in the x direction (parallel to fiber axis, arbitrary direction for myotubes). 3: Van Steensel's FWHM of Gaussian fit. 4: Li's Intensity Correlation Quotient. Definitions in Methods. p, probability of no difference between values for JPh44 and JPh1. There was no statistically significant difference between colocalization measures of the same protein in myotubes vs myofibers (p's not shown). Data and statistics in *JPh/manuscript /ColocalizJP44andRyR.JNB*.

Cytosolic/ nuclear density	GFP			FLAG		
	C2C12	Patient-derived myotubes	Murine myofibers	C2C12 myotubes	Patient-derived myotubes	Murine myofibers
avg	2.32	3.13	139	0.84	1.44	0.15
median	2.47	2.62	45.5	0.87	1.4	0.09
sem	0.47	0.59	38.5	0.12	0.26	0.03
N, n, nn	1, 3, 6	1,4, 38	3, 16, 20	1, 3, 6	1,4, 38	3, 16, 20
P				0.039	0.028	<0.001

Table 2. Fate of doubly tagged protein GFP (N) – JPh1 – FLAG (C). Distribution of GFP (N terminal) and FLAG (C-terminal) in different preparations, quantified by the ratio of densities in extranuclear ("cytosol") and nuclear areas. N, numbers of culture experiments, patients or mice. n, numbers of images. nn, numbers of nuclei included in calculations. p, probability of no difference between GFP and FLAG distributions in 2-tailed t tests. To

correct for data clustering (or pseudoreplication), average and dispersion parameters in mouse myofibers were derived by hierarchical analysis. Raw data listed in depository under the following identifiers: C2C12: 091620a. Series 2, 5, 7. Patient-derived myotubes: 091020a. Series 1-4. Mice: 092420a, 100520a, 100520b. All series. Murine in *summary flag-gfp.JNB*. Patient in *ColocalizJP44and RyR.JNB* in JPh/Manuscript Data2.

		R	VS shift, nm		FWHM, µm	ICQ	N, subjects n, stacks
			longitudinal	transversal			
JPh1 vs calpain	mean	0.718	31.67	44.67	0.63	0.297	3 9
	median	0.701	28.00	39.00	0.62	0.29	
	sem	0.036	6.41	6.18	0.02	0.012	
JPh44 vs calpain	mean	0.387	66.14	103.86	1.89	0.191	2 7
	median	0.42	60.00	89.00	1.30	0.2	
	sem	0.045	18.19	23.24	0.77	0.028	
	p	*<0.001	*0.151	*0.08	0.02	0.007	

Table 3. Colocalization measures of junctophilin vs calpain in patients' myofibers. p: probabilities in 2-tailed t test or * non-parametric difference of medians. images of experiments 051220, 113020, 081020 a (JPh1) & 08120b & 1201121 (JPh44). Section 3 in *colocalizationJPhRyR.JNB*

	With FLAG-calpain	Reference
Average	3.7411	1.1816
Median	3.4118	1.1839
SEM	0.3292	0.0923
P	<0.001	
Subjects, z-stacks	3, 19	4, 18

Table 4. Effect of FLAG-calpain expression on location of JPh1 antibody A (which detects full-size and 44 kDa fragment) in patient-derived myotubes. Location evaluated as ratio of nuclear/cytosolic density of antibody signal. Section 5 in *colocalizationJPhRyR.JNB.*

	N, subjects	n, cells		R	VS shift, nm	FWHM, µm	ICQ
Expressing FLAG-Cp1	2	13	avg	0.44	278	3.49	0.22
			median	0.42	130	2.24	0.23
			sem	0.05	127	0.96	0.03
Reference	2	16	avg	0.72	44	0.58	0.30
			median	0.73	48	0.52	0.30
			sem	0.03	5	0.04	0.01
			p*	<0.001	0.008	<0.001	0.023

Table 5. Effect of heterologous calpain on colocalization of JPh (detected with antibody A) and RyR1 in human-derived myotubes. p calculated by Mann-Whitney Rank Sum Test. Experiments 073020 a (calpain) & b (reference). 010422a (calpain). 010422a (reference). Data in *colocalizationJPhRyR.JNB*, Section #11.

Colocalization with RyR1		N, subjects	n, cells	R	VS shift, nm	FWHM, µm	ICQ
JPh	avg	2	10	**0.72**	**44**	**0.58**	**0.30**
	median			0.73	48	0.52	0.30
	sem			0.03	5	0.04	0.03
Cp1	avg	2	14	**0.76**	**126**	**1.13**	**0.34**
	median			0.76	120	0.95	0.36
	sem			0.03	25	0.15	0.03
	p*			0.336	0.01	<0.001	0.206

Table 6. Colocalization of JPh and calpain (Cp1) with RyR1 in human-derived myotubes expressing FLAG calpain. Patient #180 MHN. 073020a. 6 series. Data are in *ColocalizJP44 and RyR.JNB* section 9. 073020b. 9 series. 010422a, n = 4 series for calpain vs RyR, 5 series for JPh vs RyR. * p calculated by Mann-Whitney Rank Sum Test.

		n, myotubes	junctophilin			RyR1		
			in nuclei	in cytosol	nuc/cyt	in nuclei	in cytosol	nuc/cyt
Calpain-treated	average	16	52	18	**3.31**	71	115	**0.65**
	median		49	20	2.6	67	113	0.52
	SEM		5.8	2.0	0.58	8.4	9.4	0.09
untreated	average	13	82	67	**1.48**	179	330	**0.45**
	median		87	56	1.41	88	259	0.44
	SEM		12	12	0.27	84	86	0.08
	p				0.016			0.130

Table 7. Effect of incubation with calpain on nuclear content of junctophilin in patient-derived myotubes. Junctophilin imaged by fluorescence of antibody A. Entries are densities (signal within ROI/area, in units of convenience) or ratios of densities. p of no difference between density ratios calculated by the Mann-Whitney Rank Sum Test. The number of images analyzed was 9 for control and 10 for treated. The number of myotubes

per image was 1 or 2. All cultures were derived from one muscle sample (030320a, b, patient #173, MHS). Section (Calpain treatment of human muscle) in *Calpain files with correlations ER IDL.JNB.*

		n, myotubes	R	VS shift, nm	FWHM, µm	ICQ
untreated	avg	13	**0.75**	**26.4**	**0.49**	**0.34**
	median		0.78	18	0.46	0.37
	SEM		0.04	5.33	0.03	0.03
Calpain-treated	avg	16	**0.6**	**35.4**	**0.50**	**0.25**
	median		0.62	32.5	0.52	0.26
	SEM		0.05	6.01	0.01	0.02
	p		0.024	0.26	0.69	0.018

Table 8. Effect of extracellular calpain on Colocalization of JPh1 and RyR1 in patient myotubes. #173. MHH. 030330 a (Ref), b (treated). Number of z-stacks was 10 in both cases, with 1 to 3 myotubes in each. Data in *ColocalizJP44and RyR.JNB*, section 10.

		n, myotubes	JPh1 or JPh44		
			in nuclei	in cytosol	ratio nuc/cyt
Calpain-treated	average	11	379	240	**1.63**
	median		329	208	1.6
	SEM		50	31	0.17
untreated	average	10	541	771	**0.7**
	median		540	756	0.7
	SEM		55	21	0.07
	p				< 0.001

Table 9. Effect of extracellular calpain on C2C12 myotubes expressing (N) Myc JPh1. Junctophilin (both JPh1 and JPh44) detected by antibody A. 032720a (treated) and 032720b (untreated). N = 8 and 7 image stacks with 1 to 3 myotubes per stack. Data in *colocalizationJPhRyR.JNB.* section 4.

		N subjects	n fibers	R	VS shift, nm	FWHM,	ICQ
JPh1	average	3	8	**0.88**	**16**	**0.42**	**0.4**
	median			0.9	12	0.40	0.42
	S.E.M.			0.03	3	0.07	0.02
JPh44	average	3	10	**0.31**	**66**	**0.56**	**0.22**
	median			0.26	54	0.50	0.23
	S.E.M.			0.04	15	0.19	0.02
	p			<0.001	<0.001	0.06	<0.001
GFP-Δ(1-240) JPh1	average	1	6	**0.54**	**50**	**0.89**	**0.24**
	median			0.53	36	0.80	0.24
	S.E.M.			0.09	23	0.09	0.02
	p			0.001	0.057	<0.001	<0.001

Table 10. Colocalization of exogenous GFP-Δ(1-240) JPh1 with RyR1 in muscle of adult mice. For ease of comparison, the table includes values of JPh1 and JPh44 in human muscle, from Table 1. p of no difference between values for fragments vs. JPh1 (Mann Whitney Rank Sum for all but ICQ). Data in *ColocalizJP44andRyR.JNB*

	1	2	3	4	5	6
GSK3β density, a. u.	Cells expressing Δ construct	Cells not expressing Δ construct	Ratio col1/col2	Cells expressing GFP-EV	Cells not expressing GFP-EV	Ratio col4/col5
avg	441	729	0.62	1548	1553	1.00
median	353	547	0.61	1513	1355	1.03
sem	75.1	138	0.03	268	281	0.05
N, images	10	10	10	8	8	8
n, cells	15	73		11	42	
p			<0.001			0.958

Table 11. Effect of expression of GFP-Δ(1-240) JPh1 on density of GSK3β in C2C12 myoblasts. The reference, in Cols 4-6, is a culture transfected with the empty vector (GFP-EV). The numbers are averages of densities and their ratios calculated individually for 10 and 8 images, respectively for Δ construct and empty vector. The number of expressing cells per image varied between 1 and 3; that of non-expressing cells between 6 and 10. p is the probability of a ratio of 1, i.e., no effect of the expression, based on a 2-tailed t-test on the sample of 10 or 8 ratios. An alternative t-test (of paired differences in density between non-expressing and expressing areas) yielded a p of no difference = 0.002 and 0.930 respectively for the Δ construct and the empty vector.

Acknowledgments

We are grateful to Professor Vincenzo Sorrentino for his generous gift of an N-terminal Myc-tagged Junctophilin1 vector. Funding: National Institute of Arthritis and Musculoskeletal and Skin Diseases (R01 AR 071381) to S.R., E.R., and M. Fill (Rush University). National Institute of Arthritis and Musculoskeletal and Skin Diseases (R01 AR 072602) to E.R., S. L. Hamilton, S. Jung and F. Horrigan (Baylor College of Medicine). National Center for Research Resources (S1055024707) to E.R. and others.